ELSEVIER

International Journal of Mass Spectrometry 206 (2001) 153–176

International Journal of Mass Spectrometry

Comparative ab initio studies of heteroatom-doped carbon clusters $C_nX_p^+$ (X = P, S; $n + p = 3$–6)

G. Pascoli[a,*] and H. Lavendy[b]

Faculté des Sciences, Département de Physique AMIENS, 33 rue Saint Leu Amiens 80039 CEDEX, France
Laboratoire de Physique des Lasers, Atomes et Molécules, Villeneuve d'Ascq Centre National de la Recherche Scientifique, Centre d'études et de recherches Lasers et Applications, Université de Lille 1, Bat P5, 59655 Villeneuve d'Ascq CEDEX, France

Received 21 July 2000; accepted 30 October 2000

Abstract

Theoretical studies of $C_nX_p^+$ (X = P, S; $n + p = 3$–6) cations have been carried out. Predictions for their geometries and vibrational frequencies have been made using the B3LYP density functional method with both the 6-311G* and aug-cc-pVTZ basis sets. Relative energies have been determined at ab initio high-quality electronic correlation level of theory (CCSD(T) and CISD). A comparison of the structures and stability show that the heteroatomic $C_nX_p^+$ ($n + p = 3$, 4) clusters are unambiguously linear, except CX_3^+, for which we find a symmetric T-shaped ground-state structure with a central carbon atom. Regarding the homoatomic species, P_3^+ is predicted to be cyclic, while S_3^+ is bent, P_4^+ possesses a puckered rhombic form, and S_4^+ occurs as a square ring. When $n + p = 5$, 6, the cations $C_nX_p^+$ (X = P, S) exhibit a wide range of forms as does the ground-state geometry (except the C_nX^+ and $C_nX_2^+$ compounds, which are invariably linear with the heteroatoms at the extremities). Building-up mechanisms in medium-sized mixed phosphorus– or sulfur–carbon compounds ($n + p = 5$, 6) are then suggested. The possible structural modifications caused by the charge of the heteroatom introduced in the cluster have been also explored. (Int J Mass Spectrom 206 (2001) 153–176) © 2001 Elsevier Science B.V.

Keywords: carbon, carbon clusters, density functional theory

1. Introduction

During the past decade, much effort has been devoted to the elucidation of the structures and bonding of heteroatom-containing carbon clusters. Much of this interest is owing to, first, the development of various experimental techniques for both cluster formation and detection. For instance, mass spectrometry measurements of isolated clusters produced by laser vaporization of various carbide targets have led to the observation of a large number of anionic, for instance, C_nB^- [1] and C_nN^- [2], and cationic, as in $C_nB_p^+$ [3] and $C_nSi_p^+$ [4], species. A few chemical reactivity studies have been also devoted to $C_nSi_p^+$ clusters [5,6]. However, laboratory spectroscopy in IR and millimeter or submillimeter regions is commonly used today for identification of neutral heteroatom-doped carbon clusters like C_nSi_p [7], C_nO [8], and C_nS [9].

Second, the rapid improvement in the accuracy and

* Corresponding author. E-mail: pascoli@u-picardie.fr

PII S1387-3806(00)00385-7

the feasibility of theoretical calculations has created interest. We can especially notice the increasing efficiency and availability of density functional codes with a superior cost-to-benefit ratio relative to other ab initio methodologies for medium and large size clusters [7,10,11].

Third, the discovery of a variety of carbon clusters bonded to heteroatom-like O [12], N [13], Si [14], and S [15] in circumstellar and interstellar media has also created interest, as has the recognition in fullerene research that substitution of a carbon fullerene by a foreign atom such as B, N, Si, or S provides a unique chemical environment that may induce significant change of the electronic properties and the possibility of new types of materials [3,4].

From a theoretical point of view, neutral [16] and cationic C_nSi_p [17] clusters have received a great deal of attention, even though the fact that carbon and silicon are in the same column (IV B) of the periodic table may constitute a very special case, indeed. However, very little is known regarding carbon clusters doped with other second-row elements. However, we have shown very recently that the cluster cation series C_nP^+ [18] and C_nS^+ [19] (n = 1–20) bear strong resemblance to the corresponding sequence of C_nSi^+ cations [20]. In other words, the atomic structure, that is, the number of valence electrons, of the substitutional contaminant has only subtle effects on the ground-state geometry of pure carbon clusters doped with one single second-row atom. In binary systems, where carbons and second-row atoms are mixed in various proportions, the situation is, in contrast, much more intricate [16,17]. In the latter case, a theoretical comprehensive study appears to be eventually required. Thus, our aim is to present in this article a full survey of $C_nX_p^+$ (X = P, S; $n + p$ = 3–6) clusters in relation to $C_nSi_p^+$ species. Emphasis will be given to the possible change in geometry caused by the charge of these clusters. The purpose of this work also is to provide theoretical data such as vibrational frequencies, dipole moments, and rotational constants to aid experimentalists and astrophysicists in detecting these transient molecules.

2. Methods

The computations were performed using the GAUSSIAN94 [21] package of programs implemented on an HP 9000/770 workstation. Two types of basis have been employed: the widely used Pople's 6-311G* basis set [22] and the augmented Dunning correlation consistent valence triple ζ; (hereafter quoted as aug-cc-pVTZ) [23,24].

Methods used have been the density functional theory (DFT) with Becke's hybrid exchange functional [25]; correlation being treated through the Lee et al. functional [26] (following, it is referred to as B3LYP). Geometry optimizations for all the structures involved were made with this method by means of analytic gradient techniques. Vibrational frequencies were computed by fully analytic second-order derivatives. It has been proven that DFT/B3LYP agrees with more rigorous ab initio methods like CCSD(T) for geometries and spectra of carbon clusters but at very moderate cost [10].

We also used ab initio calculations for the accurate prediction of the relative energies on B3LYP/6-311G* geometries employing the same basis set: First, the CCSD(T) level (coupled-cluster single- and double-excitation model augmented with a noniterative triple excitation correction) [27]. This method is known to yield results close to the exact n-particle solution within the given basis set, provided the system under consideration does not exhibit significant nondynamical correlation effect [28]. Second, the configuration interaction including all single and double excitations (CISD). These calculations have been performed to assess the reliability of single-reference-based methods. We found that the weight of the reference configuration in CISD treatment in all cases exceeds 0.91 and that the coefficient for the second configuration lies in the range 0.06−0.09. This fact suggests that the species under consideration ($C_nP_p^+$ and $C_nS_p^+$) can be treated by single-reference-based computations.

Table 1
Relative energies, vibrational frequencies, Zero Point Energies (ZPE), dipole moments, and rotational constants (A, B, C) for $C_nP_p^+$ ($n + p = 3$) structures optimized with B3LYP/6-311G* method

Isomer	State	$\langle S^2 \rangle$	B3LYP/ 6-311G*	B3LYP/aug-cc-pVTZ	CCSD(T)	CISD	Vibrational frequencies (cm^{-1})	ZPE (kcal mol^{-1})	Dipole moment (Debye)	A, B, C (GHz)
C_3^+:										
I	$^2B_2$	1.02	0.0	0.0	0.0	0.0	718 (a_1) 1231 (b_2) 1663 (a_1)	5.2	0.61	52.261
										40.296
										22.753
II	$^2A_1$	0.78	3.8	4.0	2.4	8.2	598 (b_2) 1283 (a_1) 1755 (a_1)	5.2	0.53	51.512
										41.755
										23.062
III	$^2\Sigma_u^+$	0.76	8.4	9.1	3.8	15.0	124 (π_u)[d] 1228 (σ_g) 4903 (σ_u)	9.1	0.00	12.644
IV	$^4A_1'$	3.76	14.7	15.2	16.8	−0.0	1178 (a') 1178 (a') 1559 (a')	5.6	0.00	43.379
										43.379
										21.689
C_2P^+:										
V	$^1\Sigma^+$	0.00	0.0	0.0	0.0	0.0	132 (π)[d] 880 (σ) 1832 (σ)	4.2	2.37	6.422
VI	$^1A_1$	0.00	14.8	11.8	12.4	13.4	200 (b_2) 944 (a_1) 1770 (a_1)	4.2	1.62	51.744
										14.491
										11.321
VII	$^3A_2$	2.01	25.7	23.4	27.4	20.5	762 (b_2) 767 (a_1) 1539 (a_1)	4.4	0.84	47.566
										13.761
										10.674
VIII	$^3\Sigma^+$	2.06	26.9	26.1	31.5	23.9	220 (π) 309 (π) 812 (σ) 1817 (σ)	4.5	0.30	6.390
CP_2^+:										
IX	$^2\Pi_g$	0.78	0.0	0.0	0.0	0.0	185 (π_u) 260 (π_u) 622 (σ_g) 1303 (σ_u)	3.4	0.00	3.117
X	$^2A_1$	0.76	21.9	16.1	21.1	20.6	445 (a_1) 900 (b_2) 1021 (a_1)	3.4	1.03	30.571
										6.711
										5.503
XI	$^4\Sigma_u^-$	3.84	64.0	63.7	60.2	64.0	262 (π_u)[d] 583 (σ_g) 1037 (σ_u)	3.1	0.00	3.071
XII	$^2\Pi$	0.81	96.7	92.9	96.4	92.7	109i (π) 80i (π) 567 (σ) 704 (σ)	1.8	1.50	3.739
P_3^+:										
XIII	$^1A_1'$	0.00	0.0	0.0	0.0	0.0	481 (e') 481 (e') 648 (a_1')	2.3	0.00	7.322
										7.322
										3.661
XIV	$^3\Sigma_g^-$	2.13	39.5	43.5	40.1	38.5	59 (π_u)[d] 449 (σ_g) 494 (σ_u)	1.5	0.00	2.053
XV	$^3A_2$	2.06	40.8	40.5	42.5	41.0	250 (b_2) 255 (a_1) 589 (a_1)	1.6	0.24	9.418
										4.934
										3.238
XVI	$^1\Sigma_g^+$	0.00	61.7	64.3	62.3	69.8	30 (π_u) 95 (π_u) 472 (σ_g) 630 (σ_u)	1.8	0.00	2.077

[d] Degenerate frequency.

Note. B3LYP/aug-cc-pVTZ, CCSD(T) and CISD energy differences are also given, respectively, in columns 5, 6, and 7. The numbering is according to Fig. 1.

3. Results and discussion

A number of structures have been optimized for each individual cation $C_nP_p^+$ and $C_nS_p^+$. Tables 1, 2, 4, 5 list the electronic states, relative energies (at B3LYP, CCSD(T) and CISD levels), vibrational frequencies, zero-point-energy (ZPE), and rotational constants for the low-energy isomers of $C_nX_p^+$ (X = P, S; $n + p = 3$, 4) clusters. The corresponding geometries are graphically shown in Figs. 1, 2, 5, and 6. The B3LYP relative energies for the various structures of cations $C_nX_p^+$ (X = P, S; $n + p = 5$, 6) are included in Figs. 3, 4, 7, and 8. Other results for the latter species, not reported here, such as vibra-

Table 2
Relative energies, vibrational frequencies, Zero Point Energies (ZPE), dipole moments and rotational constants (A, B, C) for $C_nP_p^+$ ($n + p = 4$) structures optimized with B3LYP/6-311G* method

Isomer	State	$\langle S^2 \rangle$	B3LYP/ 6-311G*	CCSD(T)	Vibrational frequencies (cm^{-1})	ZPE (kcal mol^{-1})	Dipole moment (Debye)	A, B, C (GHz)
C_4^+:								
	$^2\Pi_g$	0.76	0.0	0.00	120 (π_u) 138 (π_u) 207 (π_g) 279 (π_g)	7.3	0.00	4.806
I					888 (σ_g) 1324 (σ_u) 2141 (σ_g)			
II	$^4\Sigma_g^-$	3.81	5.9	4.9	300*i* (π_u)[d] 450 (π_g)[d] 951 (σ_g) 1901 (σ_u) 2148 (σ_g)	8.4	0.00	5.029
III	$^2B_{1u}$	0.75	6.5	−3.2	398*i* (b_{1u}) 333 (b_{3u}) 610 (b_{2u}) 772 (a_g)	5.9	0.00	29.988
					1146 (b_{3g}) 1279 (a_g)			15.488
								10.213
IV	$^4B_1$	3.77	13.6	10.9	581 (b_1) 766 (b_2) 836 (b_2) 877 (a_1)	8.4	0.00	36.318
					1387 (a_1) 1460 (a_1)			15.708
								10.965
C_3P^+:								
V	$^3\Sigma^+$	2.05	0.0	0.0	98 (π)[d] 330 (π)[d] 658 (σ) 1255 (σ) 1997 (σ)	6.8	2.45	2.743
VI	$^1\Sigma^+$	0.00	18.3	11.8	108 (π) 168 (π) 281 (π) 448 (π) 681 (σ) 1288 (σ) 2000 (σ)	7.1	2.69	2.749
VII	$^3B_1$	2.01	20.5	12.3	419 (b_1) 430 (b_2) 623 (a_1) 901 (a_1)	7.3	0.78	36.726
					1131 (b_2) 1597 (a_1)			6.484
VIII	$^1A_1$	0.00	32.7	29.8	240*i* (b_1) 375 (b_2) 686 (a_1) 1007 (a_1)	6.2	3.61	36.731
					1035 (b_2) 1271 (a_1)			6.485
								5.512
$C_2P_2^+$:								
IX	$^2\Pi_g$	0.76	0.0	0.0	150 (π_u) 166 (π_u) 421 (π_g) 480 (π_g) 550 (σ_g) 1172 (σ_u) 1810 (σ_g)	6.8	0.00	1.558
X	$^2B_1$	0.76	29.1	22.9	295 (b_1) 396 (b_2) 547 (a_1) 902 (b_2)	5.9	0.00	39.396
					962 (a_1) 1061 (a_1)			3.223
								2.980
XI	$^4\Pi_u$	3.78	32.2	34.3	131 (π_u) 140 (π_u) 289 (π_g) 376 (π_g) 479 (σ_g) 808 (σ_u) 1996 (σ_g)	6.0	0.00	1.473
XII	$^2B_1$	0.75	51.5	50.4	112 (b_2) 234 (b_1) 506 (a_1) 584 (b_2)	5.3	2.49	7.532
					712 (a_1) 1539 (a_1)			5.715
								3.250
CP_3^+:								
XIII	$^1A_1$	0.00	0.0	0.00	112 (b_2) 325 (b_1) 427 (a_1) 441 (b_2)	4.6	0.12	8.050
					669 (a_1) 1213 (a_1)			2.434
								1.869

(continued on next page)

Table 2 (*continued*)

Isomer	State	$\langle S^2 \rangle$	B3LYP/ 6-311G*	CCSD(T)	Vibrational frequencies (cm^{-1})	ZPE (kcal mol^{-1})	Dipole moment (Debye)	A, B, C (GHz)
XIV	$^3A_2$	2.01	11.6	13.2	203 (b_2)288 (b_1)413 (a_1)	4.6	1.08	7.341
					584 (a_1)			
					678 (b_2)1046 (a_1)			2.433
								1.827
XV	$^1\Sigma^+$	0.00	18.1	17.4	63 (π)[d]247 (π)[d]457 (σ)	4.9	0.37	1.171
					855 (σ)1490 (σ)			
XVI	$^1A_1$	0.00	39.5	39.6	238 (e)[d]313 (a_1)885 (e)[d]	5.0	0.22	4.835
					912 (a_1)			
								4.835
								2.675
P_4^+:								
XVII	$^2B_1$	0.79	0.0	0.0	238 (a_1)301 (a_2)314 (a_1)	3.2	0.64	4.354
					439 (b_1)			
					441 (b_2)530 (a_1)			2.900
								2.012
XVIII	$^2B_2$	0.77	15.3	14.7	89 (b_1)105 (b_2)354 (a_1)	3.1	0.50	7.454
					417 (b_2)553 (a_1)			
					682 (a_1)			1.589
								1.310
XIX	$^4B_{1u}$	3.76	25.0	24.0	166 (b_{3u})271 (a_g)300 (b_{2u})	3.0	0.00	4.547
					372 (b_{1u})			
					486 (b_{3g})491 (a_g)			2.818
								1.739
XX	$^2A_2$	0.77	26.6	38.0	355i (b_1)207 (b_2)276 (b_2)	2.8	0.00	6.112
					415 (a_1)			
					519 (a_1)538 (a_1)			2.528
								1.788

[d] Degenerate frequency.

Note. CCSD(T) energy differences are given in column 5. The numbering is according to Fig. 2.

tional frequencies and rotational constants are available on request.

A. The $C_nP_p^+$ compounds

The C_2P^+ cation is predicted to be unambiguously linear ($^1\Sigma^+$, structure V) with one CC double bond, ~1.33 Å, and one CP double bond, ~1.58 Å. The phosphorus bears the extra charge, and the submolecule C_2 is quasineutral. On the contrary for C_2Si^+, Lavendy et al. [29] have found that the linear and cyclic isomers are energetically close to each other with insignificant energy separation of 0.1 kcal mol^{-1} at MRCI level. This illustrates a distinct valence structure effect in C_2X^+ depending on whether the heterotaom X is Si or P (Si and C share the same valence structure, while P, on the right of Si in the periodic table, has one additional electron). A similar conclusion can be made when comparing CP_2^+ and CSi_2^+. As a matter of fact, we know that CSi_2^+ is predicted to be cyclic but with an energetic separation to the linear of 0.5 kcal mol^{-1} at MRCI level [29]. Once again, as for C_2Si^+, this cation seems to hesitate between cyclic or linear geometry for its ground state. Besides, the lowest-energy CP_2^+ isomer (structure IX) is unambiguously the linear arrangement of nuclei in the $^2\Pi_g$ electronic state. Two double CP bonds (~1.62 Å) are formed, and the carbon atom is in central position. The cyclic isomer ($^2A_1$, structure X) is located above the linear one, (structure IX) respectively, by ~21.9 kcal mol^{-1} at B3LYP and 21.1 kcal mol^{-1} at CCSD(T) levels. The latter structure is a

Table 3. Building-up patterns of the $C_nP_p^+$ ($n + p = 5, 6$) clusters in their ground state. The various structures, optimized with the B3LYP/6-311G* method are reproduced in Figs. 3 and 4.

	ΔE_b (eV)
CP_2^+(linear, $^2\Pi_g$) + CP($^2\Sigma^+$) ← $C_2P_3^+$(X, $^1A'$)	5.38
C_2P(linear, $^2\Pi$) + P_2($^1\Sigma_g^+$) ↔ $C_2P_3^+$(X, $^1A'$)	4.23
CP_2(linear, $^3\Sigma_g^-$) + P_2^+($^2\Sigma_g^+$) ↔ CP_4^+(XIV, $^2B_1$)	3.31
P_3^+(cyclic, $^1A_1'$) + P_2($^1\Sigma_g^+$) ↔ P_5^+(XVIII, $^1A_1$)	1.48
$C_3P_2^+$(linear, $^2\Pi_u$) + P(^{4}S) ↔ $C_3P_3^+$(XII, $^1A_1$)	3.31
CP_2(linear, $^3\Sigma_g^-$) + CP_2^+(linear, $^2\Pi_g$) ↔ $C_2P_4^+$(XVI, ^2A_u)	3.00
CP($^2\Sigma^+$) + P_4^+(puckered rhombus, $^2B_1$) ↔ CP_5^+(XX, $^1A'$)	4.50
CP_3^+(T-shaped, $^1A_1$) + P_2($^1\Sigma_g^+$) ↔ CP_5^+(XX, $^1A'$)	1.56
P_3^+(cyclic, $^1A_1'$) + P_3(linear, $^2\Pi_g$) ↔ P_6^+(XXIV, ^2A_g)	2.59

Note. B3LYP/6-311G* total energies for P(^{4}S), $E = -341.280483$; CP($^2\Sigma^+$), $E = -379.328445$; CP^+($^3\Pi$), $E = -378.928684$; CP_2($^3\Sigma_g^-$), $E = -720.788533$; CP_2^+($^2\Pi_g$), $E = -720.464572$; C_2P($^2\Pi$), $E = -417.411929$; P_2($^1\Sigma_g^+$), $E = -682.734019$; P_2^+($^2\Sigma_g^+$), $E = -682.335715$. ΔE_b denotes the binding energy of the cluster viewed as composed of two submolecules listed in the first column.

local minimum (all real frequencies) on the CP_2^+ energy surface. The next species in the $C_nP_p^+$ sequence is P_3^+. This time, the linear-cyclic energy ordering is reversed, and this cation is clearly cyclic in its ground state ($^1A_1'$, structure XIII), lying ~39.5 kcal mol^{-1} at B3LYP and 40.1 kcal mol^{-1} at CCSD(T) levels under the linear $^3\Sigma_g^-$. It is worthy to note that P_3^+ is a perfect equilateral triangle ($^1A_1'$, structure XIII) with an equal charge (+e/3) distributed on each phosporus. We can notice that compared to the linear, the cyclic configuration has one additional PP bond. The building up of the tetra-atomic structures (Fig. 2) from the triatomic ones (Fig. 1) is straightforward. The ground-state geometries of the cations C_3P^+ ($^3\Sigma^+$, structure V) and $C_2P_2^+$ ($^2\Pi_g$, structure IX) are derived from the linear C_2P^+ ($^1\Sigma^+$, structure V) by, respectively, adding either a carbon or a phosphorus atom to the CC moiety. One way to build up CP_3^+ is to add a phosphorus to the linear CP_2^+. Proceeding like this, however, leads to a linear cluster with one PP double bond, which is found to be energetically less favorable than a CP bond. Another pathway is, thus, to start from the cyclic CP_2^+. This time, sticking a supplementary phosphorus to carbon gives a T-shaped configuration ($^1A_1$, structure XIII) with three CP bonds. In the latter structure, the carbon atom is negatively charged and the three phosphorus atoms around it are positively charged with quasiequal charges (Fig. 2), minimizing the electrostatic energy. The T-shaped CP_3^+ is located under the linear by ~18.1 kcal mol^{-1} at B3LYP and 17.4 kcal mol^{-1} at CCSD(T) levels, respectively. Both of these isomers, with all real frequencies, are local minima on the CP_3^+ energy surface. A very similar operation can be performed on P_3^+ and leads to a T-shaped P_4^+. However, this isomer is found to be less stable than the puckered rhombus ($^2B_1$, structure XVII) by 15.3 kcal mol^{-1} at the B3LYP level and 14.7 kcal mol^{-1} at the CCSD(T) level. We can notice that in the case of the neutral P_4, a tetrahedral configuration was predicted for the ground state [30]. This indicates that the extra charge destabilizes the T_d arrangement of nuclei toward a lower symmetry (C_{2v}). Such a symmetry breaking was already encountered in C_nSi_p clusters [17].

Some general remarks for the energetics in $C_nP_p^+$ compounds can be deduced from Tables 1 and 2. First, we can notice the good agreement between B3LYP and CCSD(T) energy differences for the heteroatomic clusters with maximal energy deviation systematically <10 kcal mol^{-1} between these two levels of energy computation. However, B3LYP seems to be less dependable for the evaluation of relative energies in the homoatomic species. As has

Table 4
Relative energies, vibrational frequencies, Zero Point Energies (ZPE), dipole moments and rotational constants (A, B, C) for $C_nS_p^+$ ($n + p = 3$) structures optimized with B3LYP/6-311G* method

Isomer	State	$\langle S^2 \rangle$	B3LYP/ 6-311G*	B3LYP/aug -cc-pVTZ	CCSD(T)	CISD	Vibrational frequencies (cm^{-1})	ZPE (kcal mol^{-1})	Dipole moment (Debye)	A, B, C (GHz)
C_2S^+:										
I	$^2\Pi$	0.76	0.0	0.0	0.0	0.0*	182 (π) 252 (π) 858 (σ) 1577 (σ)	4.1	1.11	6.422
II	$^4\Sigma^-$	3.81	1.3	1.3	3.0	14.6*	360 (π) 905 (σ) 1701 (σ)	4.7	1.35	6.667
III	$^2B_2$	0.75	27.9	25.0	29.4	51.0*	637i (b_2) 857 (a_1) 1393 (a_1)	3.2	1.16	44.958 15.338 11.436
IV	$^4A_2$	3.76	35.0	40.0	36.0	51.9*	480 (b_2) 699 (a_1) 1668 (a_1)	4.1	0.33	49.862 12.807 10.190
CS_2^+:										
V	$^2\Pi_g$	0.78	0.0	0.0	0.0	0.0	314 (π_u) 365 (π_u) 667 (σ_g) 1247 (σ_u)	3.7	0.00	3.251
VI	$^2A_2$	0.77	65.7	58.4	63.9	65.0	407 (b_2) 564 (a_1) 837 (a_1)	2.6	1.41	23.554 7.581 5.735
VII	$^4\Pi_g$	3.78	77.8	76.3	80.5	76.1	422i (π_u) 250 (π_u) 580 (σ_g) 1282 (σ_u)	3.0	0.00	3.041
VIII	$^4B_2$	3.76	103.8	96.8	103.7	93.3	494 (a_1) 752 (b_2) 913 (a_1)	3.1	0.42	26.276 7.219 5.663
S_3^+										
IX	$^2B_2$	0.76	0.0	0.0	0.0	0.0	209 (a_1) 441 (b_2) 598 (a_1)	1.8	0.60	15.445 3.435 2.810
X	$^4A_1$	3.76	7.0	9.6	9.3	8.0	215 (a_1) 410 (b_2) 564 (a_1)	1.7	0.00	10.150 4.173 2.957
XI	$^2\Sigma_g^+$	0.76	31.3	32.2	30.3	33.6	976i (π_u)[d] 431 (σ_g) 492 (σ_u)	1.3	0.00	2.059
XII	$^4\Sigma_u^+$	3.91	56.0	54.2	50.1	54.8	550i (π_u) 465i (σ_u) 154 (π_u) 326 (σ_g)	0.7	0.00	1.780

* Geometry optimized at CISD level.
[d] Degenerate frequency.
Note. B3LYP/Aug-cc-pVTZ, CCSD(T) and CISD energy differences are also given, respectively in columns 5, 6 and 7. The numbering is according to Fig. 5.

already been noticed for C_4^+ [31], the energy order for the linear $^2\Pi_g$ and cyclic $^2B_{1u}$ isomers found at B3LYP is reversed at CCSD(T) level. But these two isomers are energetically close to each other (energy separation of the order of 6 kcal mol^{-1} at B3LYP level in favor of the linear and 3 kcal mol^{-1} in favor of the cyclic at the CCSD(T) level of theory). For such a critical case, the CCSD(T) energies have to be considered more reliable than B3LYP ones [11].

Another major point of our study concerns the deduction of the building-up patterns operative for large phosphorus–carbon clusters. This important element can be extracted from an analysis of the two consecutive sequences C_5^+, C_4P^+, . . . , P_5^+ and C_6^+, C_5P^+, . . . , P_6^+ when C is gradually replaced by P (Figs. 3, 4; Table 3). A general rule is that CC bonds are favored over CP bonds and PP bonds are—if possible—avoided to arrange the structures in a minimal energy state. A very similar conclusion was made by Froudakis et al. concerning the C_nSi_p clus-

Table 5
Relative energies, vibrational frequencies, Zero Point Energies (ZPE), dipole moments and rotational constants (A, B, C) for $C_nS_p^+$ ($n + p = 4$) structures optimized with B3LYP/6-311G* method

Isomer	State	$\langle S^2 \rangle$	B3LYP/ 6-311G*	CCSD(T)	Vibrational frequencies (cm^{-1})	ZPE (kcal mol^{-1})	Dipole moment (Debye)	A, B, C (GHz)
C_3S^+:								
I	$^2\Pi$	0.78	0.0	0.0	154 (π) 190 (π) 453 (σ) 536 (Π) 725 (σ) 1363 (σ) 1890 (σ)	7.6	1.58	2.834
II	$^2B_1$	0.77	35.4	32.7	472*i* (b_2) 430 (b_2) 674 (a_1) 960 (b_1) 1206 (a_1) 1540 (a_1)	6.9	0.74	48.337 4.366 4.004
III	$^2A_1$	0.76	43.7	37.4	343 (b_2) 374 (b_1) 652 (a_1) 957 (a_1) 1028 (b_2) 1686 (a_1)	7.2	0.07	37.114 6.779 5.732
IV	$^4\Sigma^+$	3.80	46.4	57.7	107 (π) 184 (π) 376 (π) 435 (π) 696 (σ) 1335 (σ) 1981 (σ)	7.3	1.85	2.832
$C_2S_2^+$:								
V	$^2\Pi_u$	0.75	0.0	0.0	176 (π_u) 185 (π_u) 361 (π_g) 516 (π_g) 579 (σ_g) 1330 (σ_u) 1900 (σ_g)	7.2	0.00	1.598
VI	$^4\Pi_g$	3.76	41.7	44.6	157 (π_u) 164 (π_u) 284 (π_g) 336 (π_g) 520 (σ_g) 812 (σ_u) 1053 (σ_g)	6.2	0.00	1.520
VII	$^2A_2$	0.76	102.8	100.0	134 (b_2) 251 (b_1) 409 (b_2) 526 (a_1) 696 (a_1) 1679 (a_1)	5.3	2.64	7.713 5.694 3.276
VIII	$^2B_2$	0.76	105.6	99.8	474*i* (b_1) 192 (b_2) 398 (a_1) 472 (b_2) 788 (a_1) 877 (a_1)	3.9	0.00	34.028 3.249 2.966
CS_3^+:								
IX	$^2B_{2u}$	0.76	0.0	0.0	213 (b_2) 323 (b_1) 341 (b_2) 456 (a_1) 604 (a_1) 1299 (a_1)	4.6	2.01	7.441 2.529 1.887
X	$^4\Sigma^+$	3.76	25.3	26.1	150 (π)[d] 94 (σ) 289 (π)[d] 662 (σ) 1464 (σ)	4.0	2.94	0.857
XI	$^2\Pi$	0.77	44.1	51.0	550*i* (π) 434*i* (π) 198 (π) 205 (π) 332 (σ) 726 (σ) 1530 (σ)	4.3	0.06	1.142
XII	$^4A_1$	3.76	50.2	52.4	379*i* (b_1) 206 (b_2) 423 (a_1) 585 (b_2) 594 (a_1) 1115 (a_1)	4.2	1.76	7.622 2.408 1.830
S_4^+:								
XIII	$^2B_1$	0.75	0.0	0.0	72 (^b2_u) 304 (^b1_g) 450 (e_u) 450 (e_u) 497 (^a1_g) 541 (^b2_g)	3.3	0.00	3.543 3.538 1.770
XIV	$^2A_1$	0.78	7.8	6.4	82 (a_1) 153 (a_2) 234 (b_2) 251 (a_1) 613 (b_2) 671 (a_1)	2.9	0.13	11.279 1.182 1.070
XV	$^2\Pi_u$	0.77	20.2	16.9	76*i* (π_u) 62*i* (π_u) 143 (σ_g) 152 (π_g) 221 (π_g) 715 (σ_u) 731 (σ_g)	2.8	0.00	0.662
XVI	$^2B_2$	0.75	28.1	26.1	257 (a_1) 304 (a_1) 318 (b_2) 323 (a_2) 413 (b_1) 512 (a_1)	3.1	0.19	3.985 2.947 2.067

[d] Degenerate frequency.
Note. CCSD(T) energy differences are given in column 5. The numbering is according to Fig. 6.

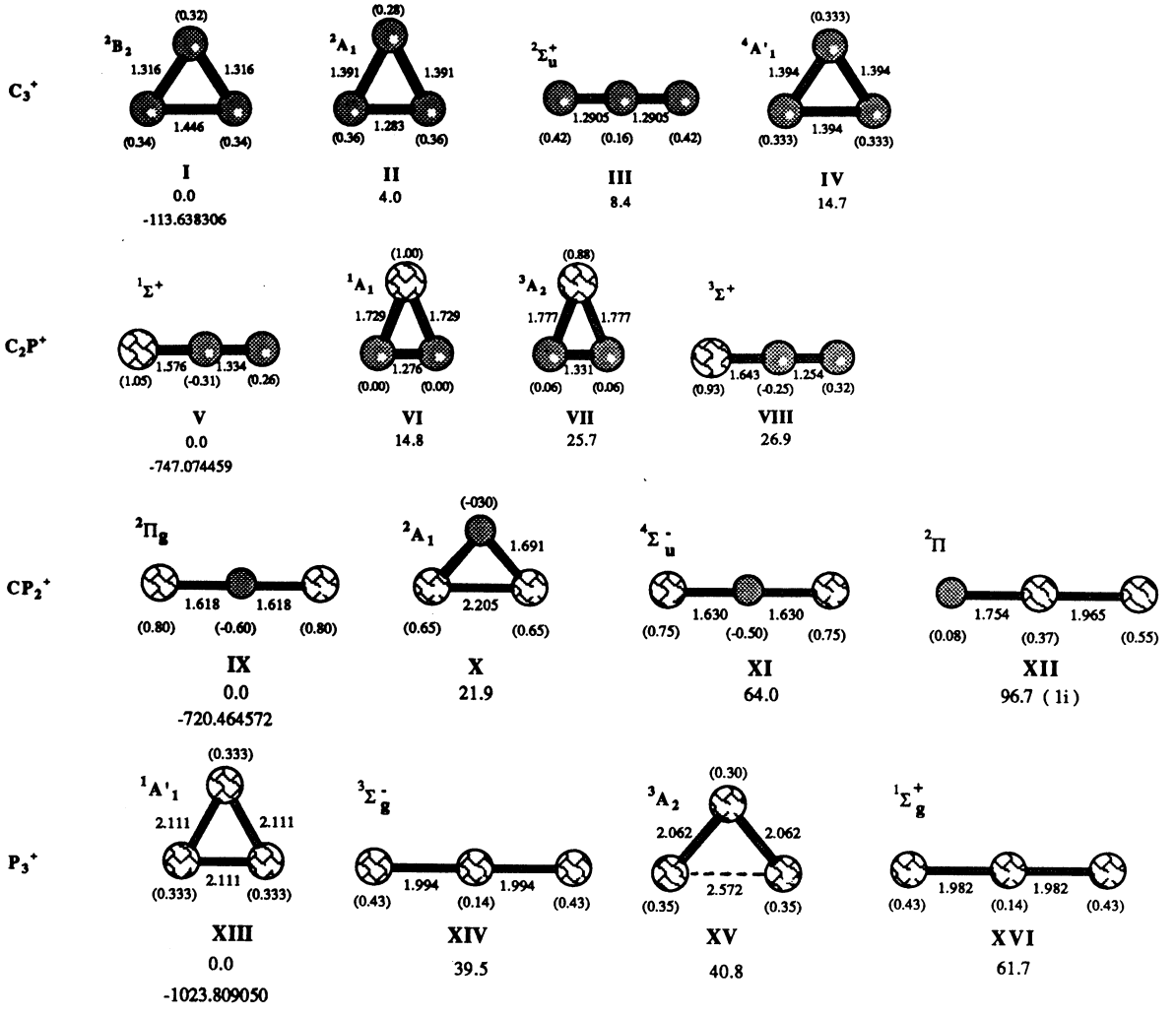

Fig. 1. Equilibrium geometries of $C_nP_p^+$ ($n + p = 3$) clusters at the B3LYP/6-311G* level of theory. Distances are in Ångstroms and angles in degrees. Mulliken charge distributions are given in parentheses. B3LYP relative energies (in kcal mol^{-1}) are displayed under each structure together with some features about the vibrational frequencies (*r* indicates that all the frequencies are real, *i* notices one imaginary frequency, 2*i* two imaginary frequencies, etc.). B3LYP/6-311G* total energies (in hartree) are also reported under the global minimum of each compound.

ters [16]. When $p = 1, 2$, calculations predict a cumulenic linear structure for $C_nP_p^+$ ($n + p = 5, 6$) clusters with phosphorus atoms in the terminal positions. Similar ground-state geometry structures were found in the case of $C_nSi_p^+$ [17]. Conversely, as soon as p is equal or >3, the ground-state structures of $C_nP_p^+$ ($n + p = 5, 6$) drastically differ from the corresponding ones already found for $C_nSi_p^+$ [17]. As a matter of fact, phosphorus has three unpaired electrons in 3_p orbitals that are available for bonding, but the promotional energy $3s \rightarrow 3d$ is small enough to allow *d* orbitals to participate in bonding and form a number of possible hybridized orbitals with various interbond angles, which ultimately leads to many possible geometric arrangements [32].

The optimized structure of $C_2P_3^+$ ($^1A'$, structure X) appears as a T-shaped configuration with a positive charge equally distributed at the periphery, that is, on the three phosphorus atoms. By contrast, $C_2Si_3^+$ was found to be a Si-capped bent chain. As a consequence,

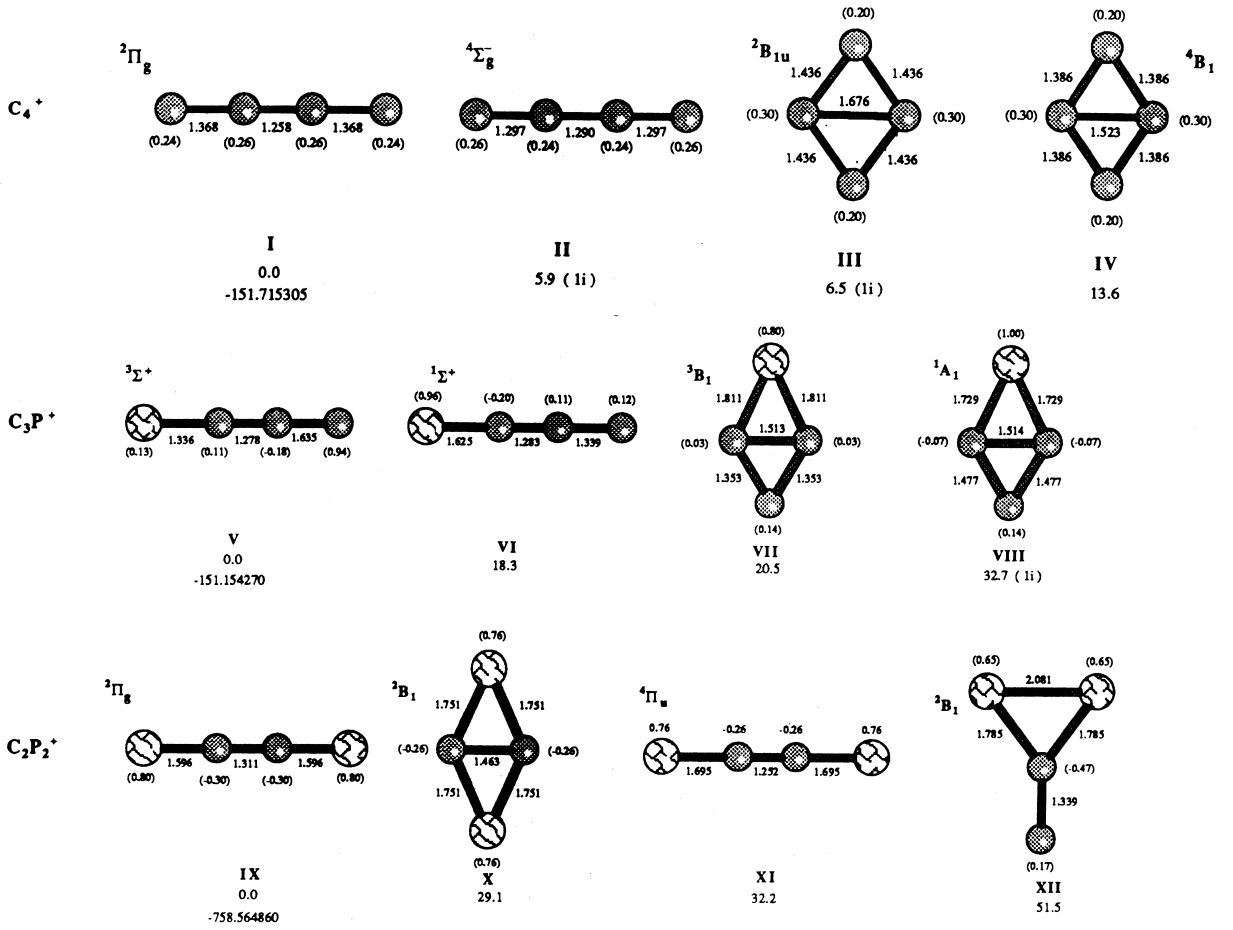

Fig. 2. Equilibrium geometries of $C_nP_p^+$ ($n + p = 4$) clusters at the B3LYP/6-311G* level of theory. Distances are in Ångstroms and angles in degrees. Mulliken charge distributions are given in parentheses. B3LYP relative energies (in kcal mol^{-1}) are displayed under each structure together with some features about the vibrational frequencies (*r* indicates that all the frequencies are real, *i* notices one imaginary frequency, 2*i* two imaginary frequencies, etc.). B3LYP/6-311G* total energies (in hartree) are also reported under the global minimum of each compound.

the building-up pattern of these two clusters radically differs. Whereas $C_2Si_3^+$ is formed by adding an Si atom perpendicularly to the median moiety (C_2 submolecule) of the linear $C_2Si_2^+$, the cation $C_2P_3^+$ ($^1A'$, structure X) is formed by placing a monopositive P_2 fragment perpendicularly to a neutral C_2P submolecule, the latter one being taken in its linear $^2\Pi$ ground state. Replacing a carbon atom by a phosphorus atom gives a planar CP_4^+ cluster ($^2B_1$, structure XIV). The corresponding CSi_4^+ cluster was found to be a C-capped quasiplanar Si_4^+ structure. Again, even though these two clusters present some likeness, distinct building-up mechanisms have to be envisaged for them. The CSi_4^+ cluster is formed by placing a carbon atom above a Si_4^+ rhombus, while CP_4^+ is formed by a cation P_2^+ attached to a CP_2 molecule in parallel. Likewise, the cation P_5^+ is found to be a tetragonal pyramid ($^1A_1$, structure XVIII) with constrained interbond angles of 60°, whereas Si_5^+ prefers a trigonal bipyramidal arrangement [17], the latter configuration being unstable for P_5^+. To the contrary, the tetragonal pyramidal arrangement was predicted to be a saddle point on the potential energy surface (PES) in the case of Si_5^+ [17]. We can still notice that,

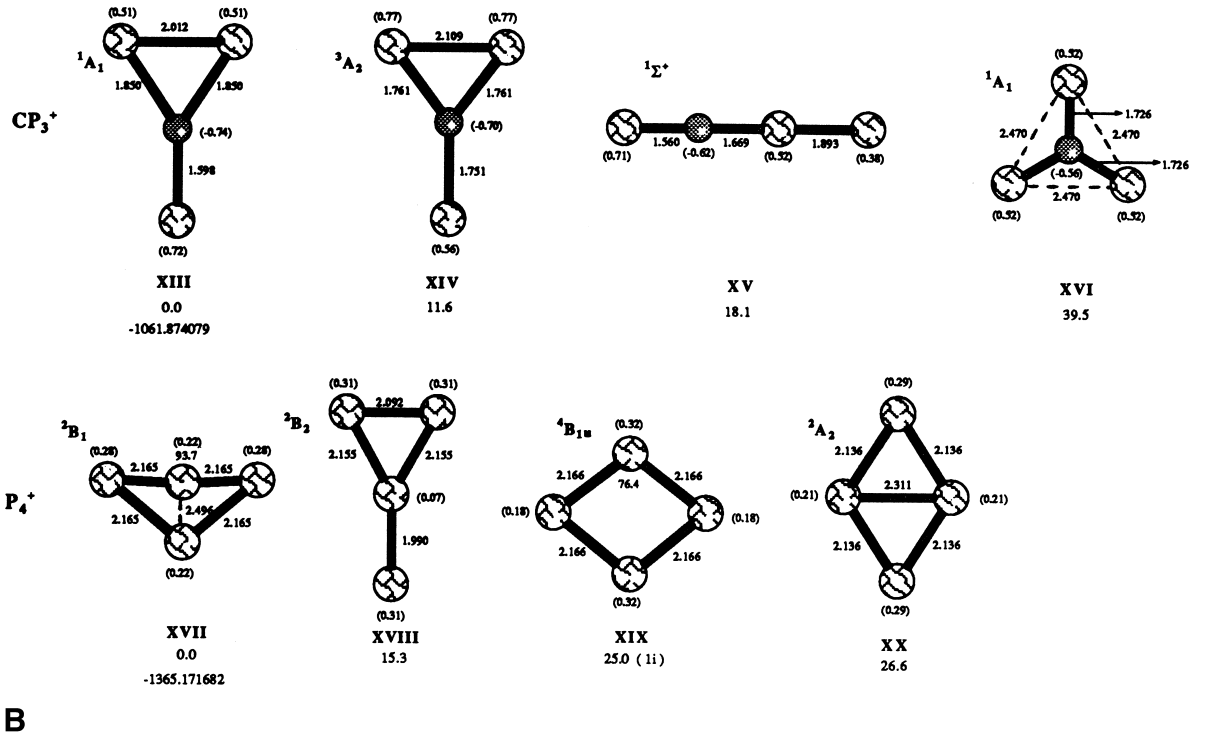

Fig. 2. (*continued*)

even though the tetragonal pyramidal configuration represents the ground-state geometry of P_5^+ (global minimum on the PES), this cation can easily be dissociated into a cation P_3^+ and a P_2 submolecule with very low fragmentation energy, of the order of 1.5 eV (Table 3). The building-up principle can also be extended to hexa-atomic clusters. The $C_3P_3^+$ cluster adopts a T-shaped configuration ($^1A_1$, structure XII). This geometry can be viewed as a C_3P linear chain with a cation P_2^+ perpendicularly attached in terminal position on the opposite side to phosphorus. The geometry of $C_2P_4^+$, namely structure XVI, is formed by association of two symmetric CP_2 submolecules strongly bound together by a double covalent CC bond with a positive charge equally distributed on the two CP_2 moieties. Comparatively, the ground-state geometry of both neutral and cationic forms of C_2Si_4 was predicted to be the C_2-capped Si_4 rhombus [17]. The latter configuration is found to be unstable for $C_2P_4^+$. Exchanging now a carbon by a silicon gives CP_5^+. The ground-state geometry of this cluster ($^1A'$, structure XX) can be viewed as a puckered four-membered ring P_4^+ capped by a CP fragment placed perpendicularly above it. However, according to the binding energies listed in Table 3, CP_5^+ appears as a T-shaped structure with three phosphorus atoms connected to a central sp^2-hybridized carbon atom, the latter planar substructure being bridged by a P_2 submolecule placed perpendicularly to its plane. Again, this geometry is different from that found in CSi_5^+, which is a Si-capped quasiplanar CSi_4^+ structure. Eventually, P_6^+, which looks like a puckered double-T-shaped arrangement of nuclei (^2A_g, structure XXIV), can be represented by two weakly interacting P_3 sharing a quasiequal positive charge. But this cation can easily dissociate into fragments P_3 and P_3^+ with low fragmentation energy of the order of 2.6 eV (Table 3). In line with this, it is worth mentioning that Si_6^+ prefers an edge-capped trigonal pyramid for its ground-state geometry [17].

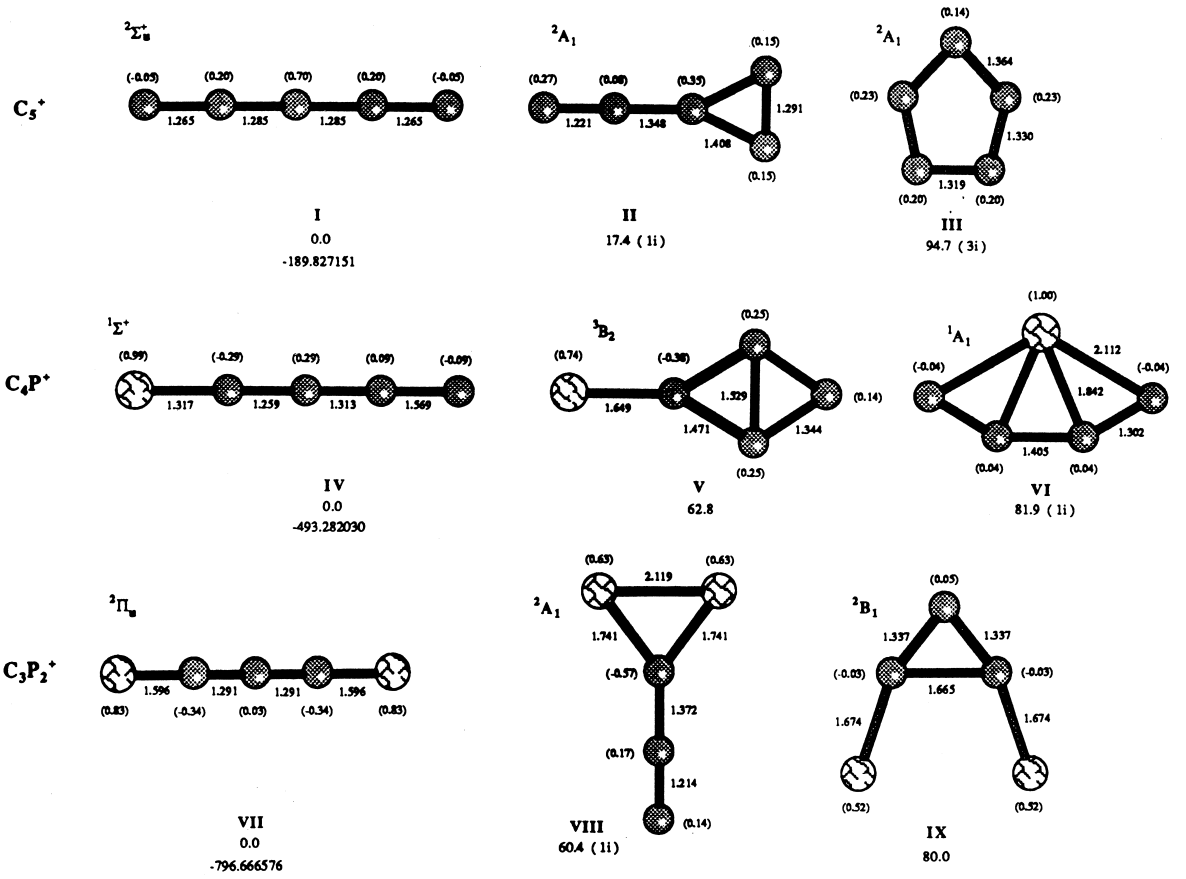

A

Fig. 3. Equilibrium geometries of $C_nP_p^+$ ($n + p = 5$) clusters at the B3LYP/6-311G* level of theory. Distances are in Ångstroms and angles in degrees. Mulliken charge distributions are given in parentheses. B3LYP relative energies (in kcal mol^{-1}) are displayed under each structure together with some features about the vibrational frequencies (*r* indicates that all the frequencies are real, *i* notices one imaginary frequency, 2*i* two imaginary frequencies, etc.). B3LYP/6-311G* total energies (in hartree) are also reported under the global minimum of each compound.

B. The $C_nS_p^+$ compounds

We consider now how the mixed heteroatom-carbon clusters evolve when phosphorus is replaced by its neighbor to the right in the periodic table, that is, by sulfur, the latter element possessing a supplementary valence electron. Once again, as for C_nP^+ and $C_nP_2^+$, the mono- and disulfide cations C_nS^+ and $C_nS_2^+$ are predicted to be cumulenic linear chains with CC and CS double bonds and S atoms in terminal positions (Figs. 5–8). This rule appears general for carbon clusters doped with one or two first-row or second-row elements. However, when three or more sulfur atoms are present in the cluster, the equilibrium structure drastically changes because of the fact that the cluster with three sulfur atoms refuses to adopt a linear geometry. For instance, the lowest-energy configuration of S_3^+ is found to be a bent chain in the $^2B_2$ electronic state (structure IX). In the latter structure, the two sulfur–sulfur bonds are ~1.96 Å, typical of relatively strong single sulfur–sulfur bonds (the sulfur–sulfur bond in H_2S_2 is predicted to be on the order

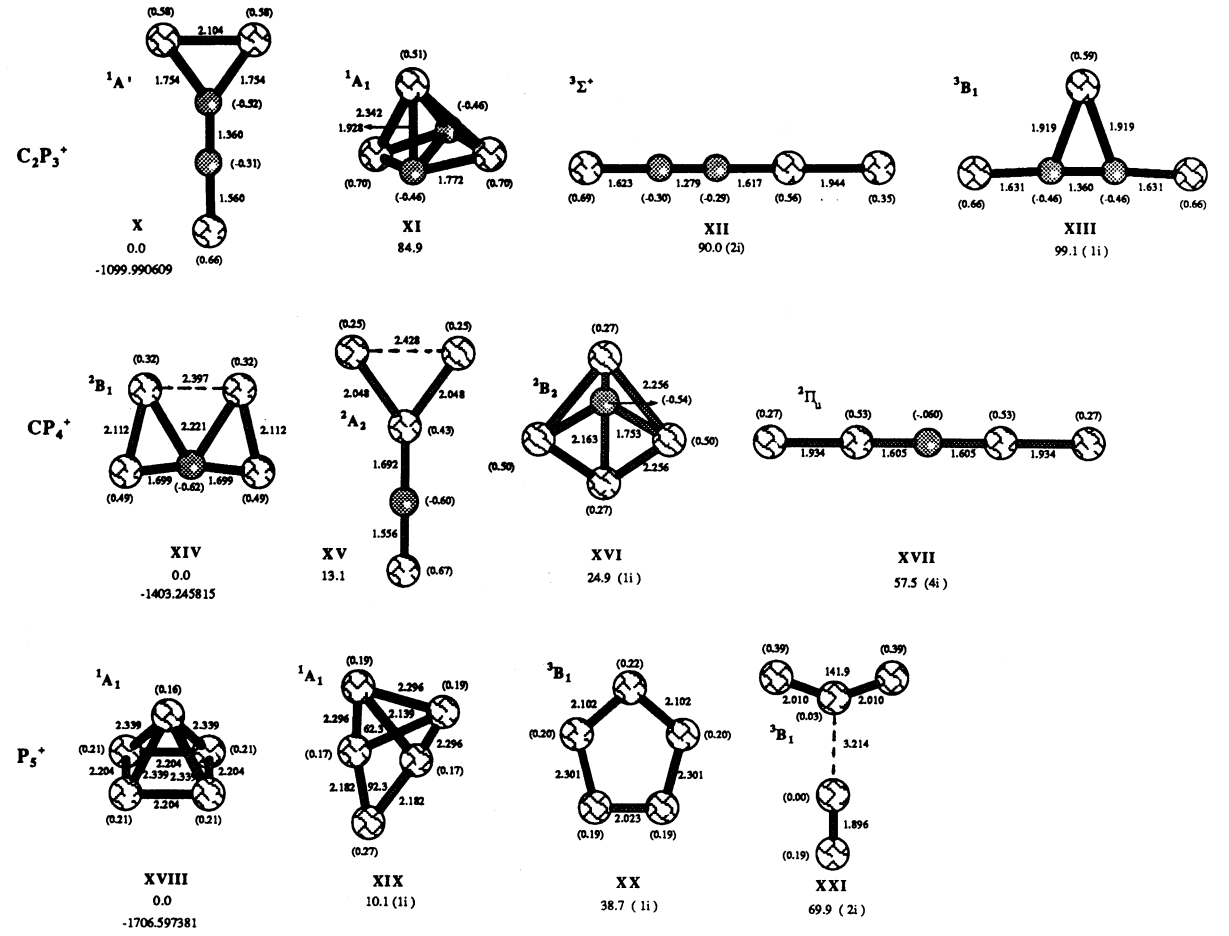

Fig. 3. (*continued*)

of 2.06 Å, [33]; in contrast to P_3^+, however, the obtuse angle of 101.5° prevents the formation of an additional sulfur–sulfur bond to close the cycle). The linear isomer ($^2\Sigma_g^+$, structure XI) is located higher in energy above the bent configuration, at 31.3 kcal mol^{-1} at B3LYP and 30.3 kcal mol^{-1} at CCSD(T) levels. Moreover, the latter structure possesses one imaginary doubly degenerated bending mode, indicating that this configuration is not a local minimum on the S_3^+ energy surface. Adding a carbon to S_3^+, we obtain CS_3^+, which adopts a T-shaped configuration for its ground state ($^2B_1$, structure IX), with a carbon atom in the central position to realize the maximum number of CS bonds, that is, two single CS bonds (∼1.80 Å) and one moderately strong double CS bond (∼1.56 Å) (Fig. 6). The corresponding linear isomer ($^4\Sigma^+$, structure X) is located at about 25.3 kcal mol^{-1} at the B3LYP level and 26.1 kcal mol^{-1} at the CCSD(T) level above the T-shaped ground state. But this structure, with two imaginary frequencies, is a saddle point of higher order on the PES. Let us notice that the hypervalent pyramidal structure (not reported on Fig. 6) is located at 128.2 kcal mol^{-1} above the absolute minimum, and the latter geometry also corrresponds to a saddle point on the PES. Adding now a sulfur atom to S_3^+ gives a S_4^+ square ring with four equivalent S atoms ($^2B_{2u}$, structure XIII). The next minimum on the PES of S_4^+ in the energetic ordering

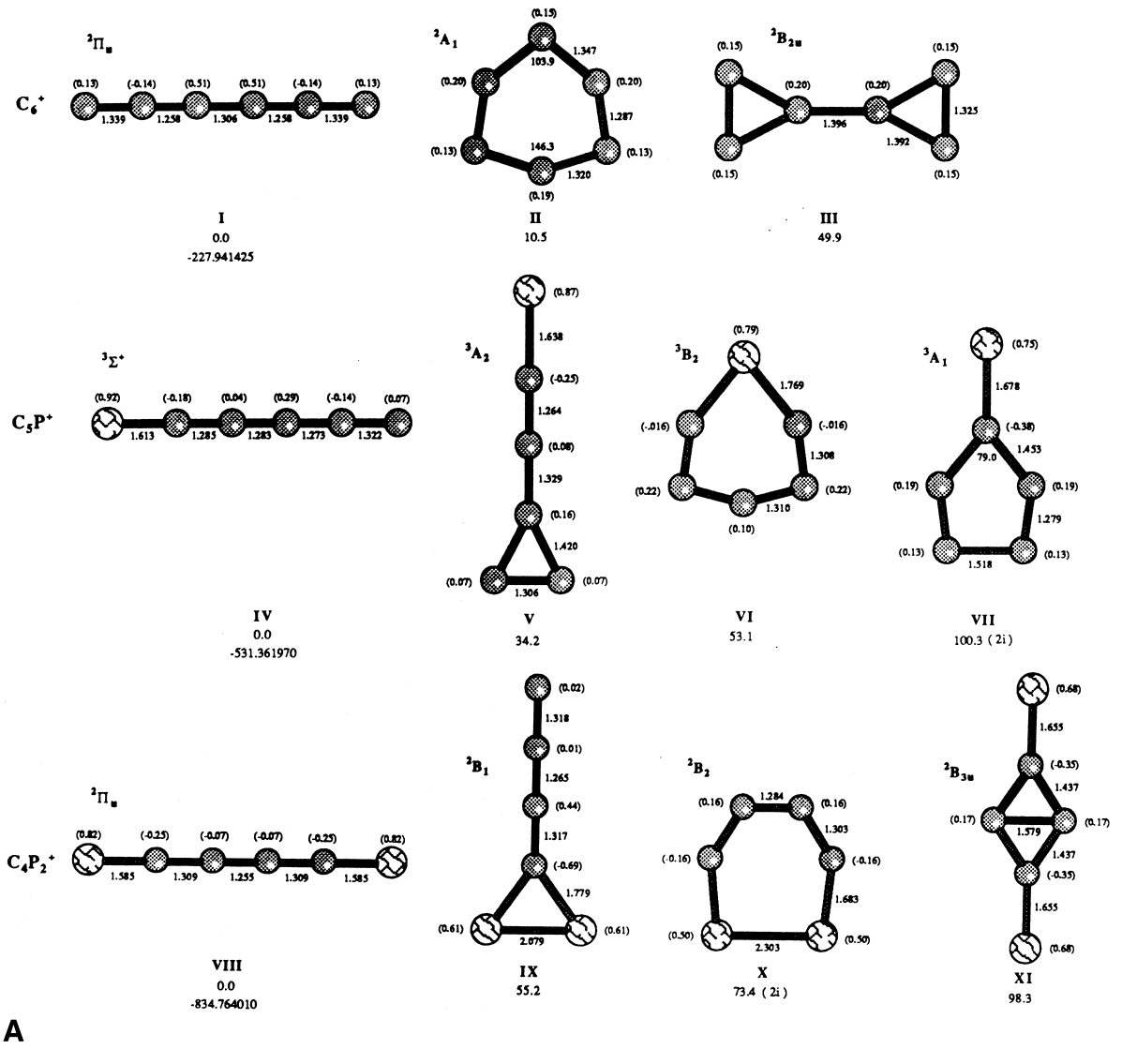

Fig. 4. Equilibrium geometries of $C_nP_p^+$ ($n + p = 6$) clusters at the B3LYP/6-311G* level of theory. Distances are in Ångstroms and angles in degrees. Mulliken charge distributions are given in parentheses. B3LYP relative energies (in kcal mol^{-1}) are displayed under each structure with some features about the vibrational frequencies (*r* indicates that all the frequencies are real, *i* notices one imaginary frequency, 2*i* two imaginary frequencies, etc.). B3LYP/6-311G* total energies (in hartree) are also reported under the global minimum of each compound.

is the cis-planar structure XIV. This open form is found to lie only ~7.8 kcal mol^{-1} above the square-ring ground state. In contrast, the corresponding linear geometry ($^2\Pi_u$, structure XV), located at 20.1 kcal mol^{-1} above the ground state, is not a minimum on the PES (two imaginary frequencies).

Regarding the energetics, as in the case of hetero-atomic $C_nP_p^+$ clusters, B3LYP and CCSD(T) energy differences for $C_nS_p^+$ are in good agreement with each other, the maximal energy deviation being on the order of 5 kcal mol^{-1} (there does, however, exist an exception in C_3S^+ where this deviation amounts to 10 kcal mol^{-1} for the relative energies of the linear quadruplet $^4\Sigma^+$ calculated with respect to the linear doublet

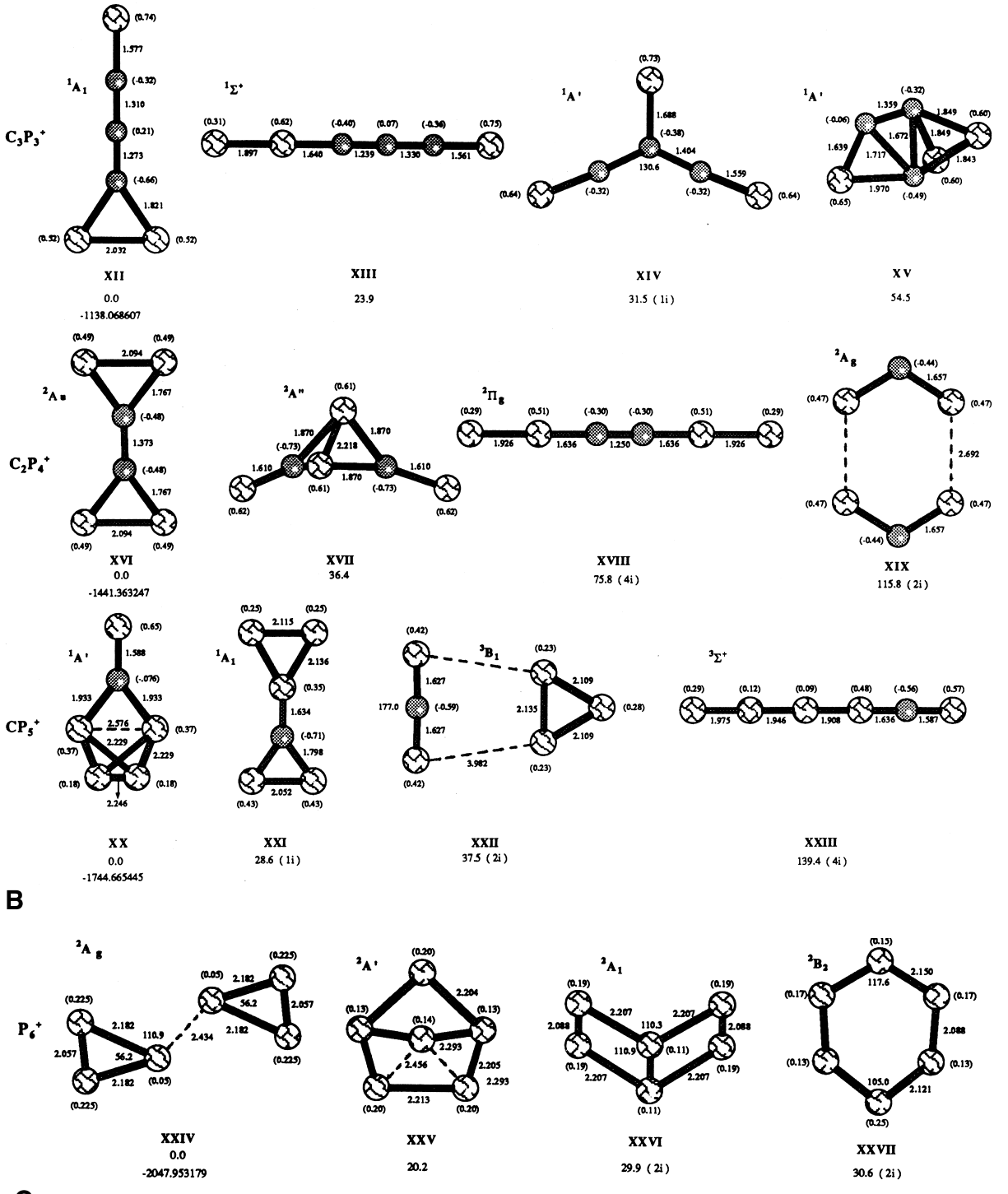

Fig. 4. (*continued*)

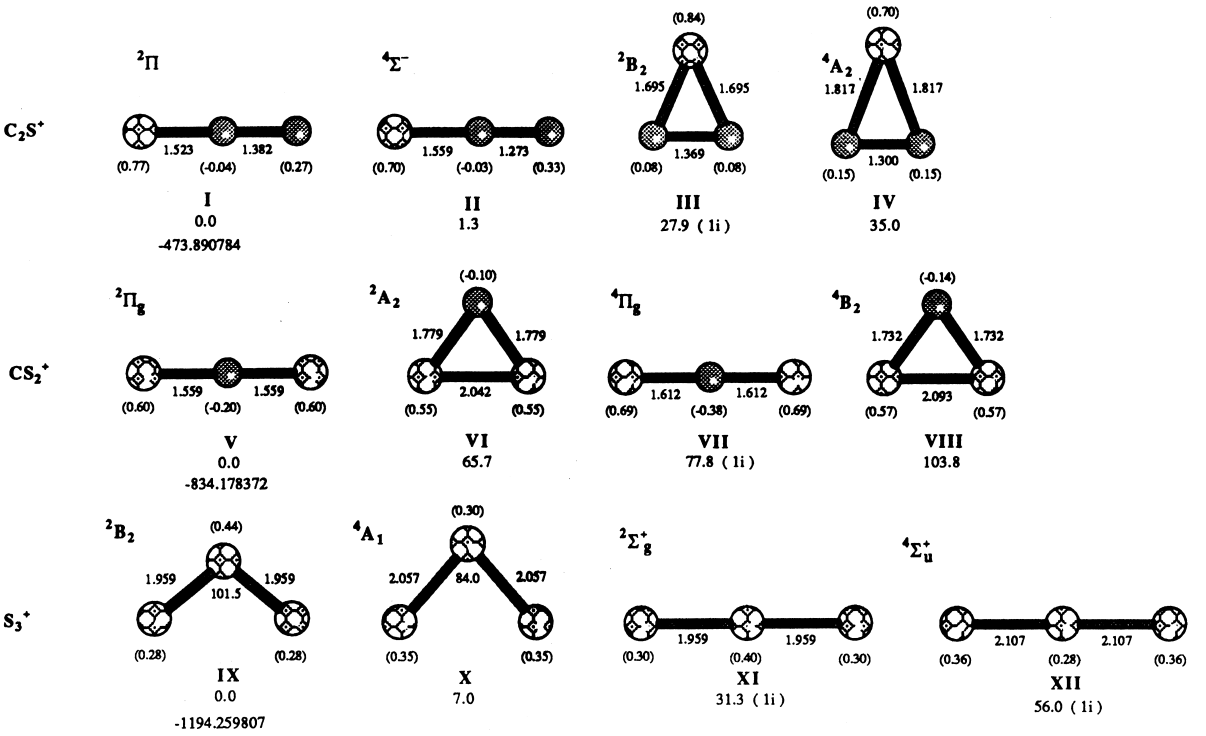

Fig. 5. Equilibrium geometries of $C_nS_p^+$ ($n + p = 3$) clusters at the B3LYP/6-311G* level of theory. Distances are in Ångstroms and angles in degrees. Mulliken charge distributions are given in parentheses. B3LYP relative energies (in kcal mol^{-1}) are displayed under each structure together with some features about the vibrational frequencies (*r* indicates that all the frequencies are real, *i* notices one imaginary frequency, 2*i* two imaginary frequencies, etc.). B3LYP/6-311G* total energies (in hartree) are also reported under the global minimum of each compound.

ground state). Comparatively, Martin et al. found much larger deviations in pure carbon clusters [11].

Special emphasis can be given to the bonding properties, especially the relationship between structure and stability for medium-sized mixed sulfur–carbon clusters, by examining the building-up mechanisms of $C_nS_p^+$ ($n + p = 5, 6$) clusters (Figs. 7, 8; Table 6). However, as is usual for second-row heteroatom-doped carbon clusters when $p = 1$ or 2, we found a linear carbon chain with heteroatoms in terminal positions as ground-state geometry. Hence, we shall only discuss here the much more interesting case where $p \geq 3$. The planar $C_2S_3^+$ cluster is composed of a cation CS_2^+ with one CS bond capped by a CS molecule. Replacing one carbon by a sulfur atom gives a Van der Waals complex (CS_4^+) composed of two quasi-independent entities, CS_2 and S_2, with equal charge distributed on them. This result demonstrates that the stability of carbon-doped sulfur molecules could indeed be relatively weak. The fragmentation energies of cations $C_nS_p^+$ ($n + p = 5, 6$) have been summarized in Table 6, where we can see that these energies are very low, mostly on the order of 1–2.6 eV. Eventually, the ground-state geometry of the pure sulfur cluster S_5^+ is a cis-trans open chain ($^2A''$, structure XV), which can readily decompose into S_3^+ and S_2 (Table 6). This structure is almost degenerate with the puckered ring ($2A'$, structure XVI), with insignificant energetic separation ~0.1 kcal mol^{-1} at B3LYP level. The corresponding cyclic planar isomer, with two imaginary frequencies, is a saddle point on the potential energy surface. Proceeding now to the hexa-atomic species (Fig. 8), the most favorable isomer of $C_3S_3^+$ is represented by a fairly stable arrangement of nuclei, where each sulfur atom is bound on the periphery of a pure carbon submol-

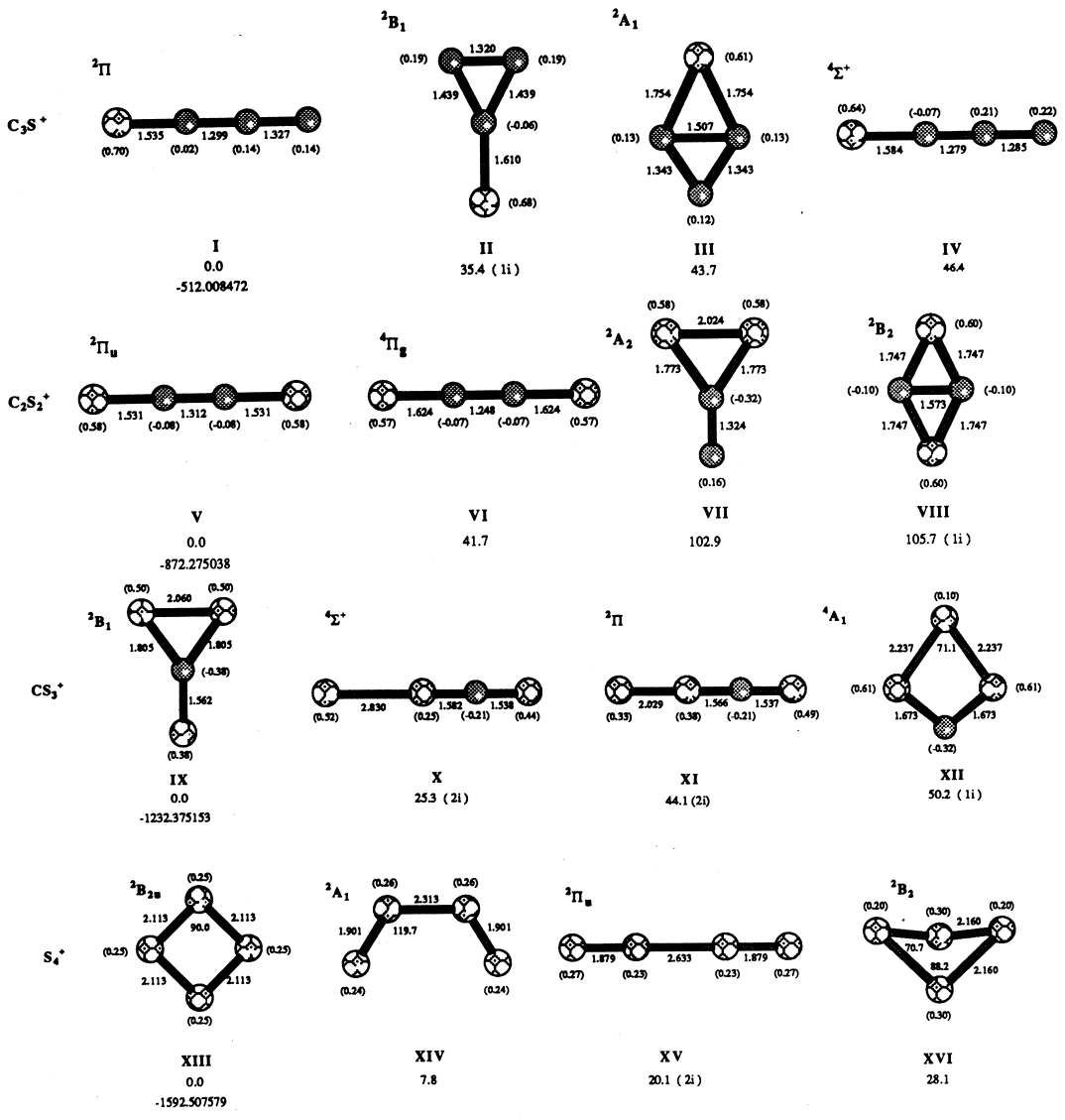

Fig. 6. Equilibrium geometries of $C_nS_p^+$ ($n + p = 4$) clusters at the B3LYP/6-311G* level of theory. Distances are in Ångstroms and angles in degrees. Mulliken charge distributions are given in parentheses. B3LYP relative energies (in kcal mol^{-1}) are displayed under each structure together with some features about the vibrational frequencies (*r* indicates that all the frequencies are real, *i* notices one imaginary frequency, 2*i* two imaginary frequencies, etc.). B3LYP/6-311G* total energies (in hartree) are also reported under the global minimum of each compound.

ecule C_3 ($^2B_1$, structure VIII). The next cluster, $C_2S_4^+$, obtained by replacing a carbon by a sulfur, is not a truly six-membered molecule but rather appears as two interacting, and equally charged, CS_2 radicals. Hence, this metastable molecule can easily dissociate into a cation CS_2^+ and the corresponding neutral (Table 6). The global minimum of CS_5^+ is predicted to be a five-membered puckered CS_4 ring with an extra SC bond ($^2A'$, structure XV), but this form is isoenergetic with the distorted chain ($^2A_1$, structure XVI), the energy separation being insignificant (on the order of 1.5 kcal mol^{-1} at the B3LYP/6-311G* level).

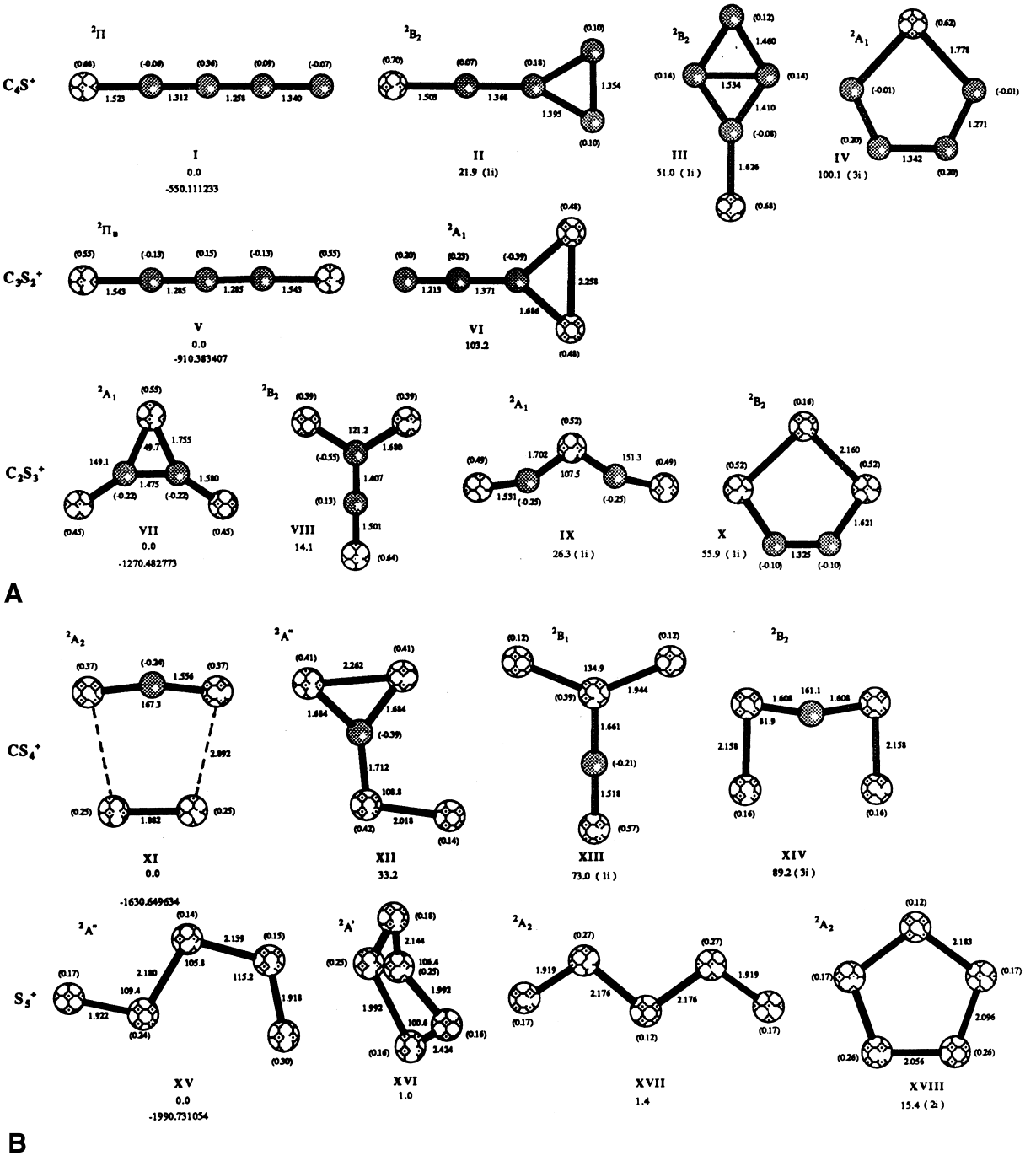

Fig. 7. Equilibrium geometries of $C_nS_p^+$ ($n + p = 5$) clusters at the B3LYP/6-311G* level of theory. Distances are in Ångstroms and angles in degrees. Mulliken charge distributions are given in parentheses. B3LYP relative energies (in kcal mol^{-1}) are displayed under each structure with some features about the vibrational frequencies (*r* indicates that all the frequencies are real, *i* notices one imaginary frequency, 2*i* two imaginary frequencies, etc.). B3LYP/6-311G* total energies (in hartree) are also reported under the global minimum of each compound.

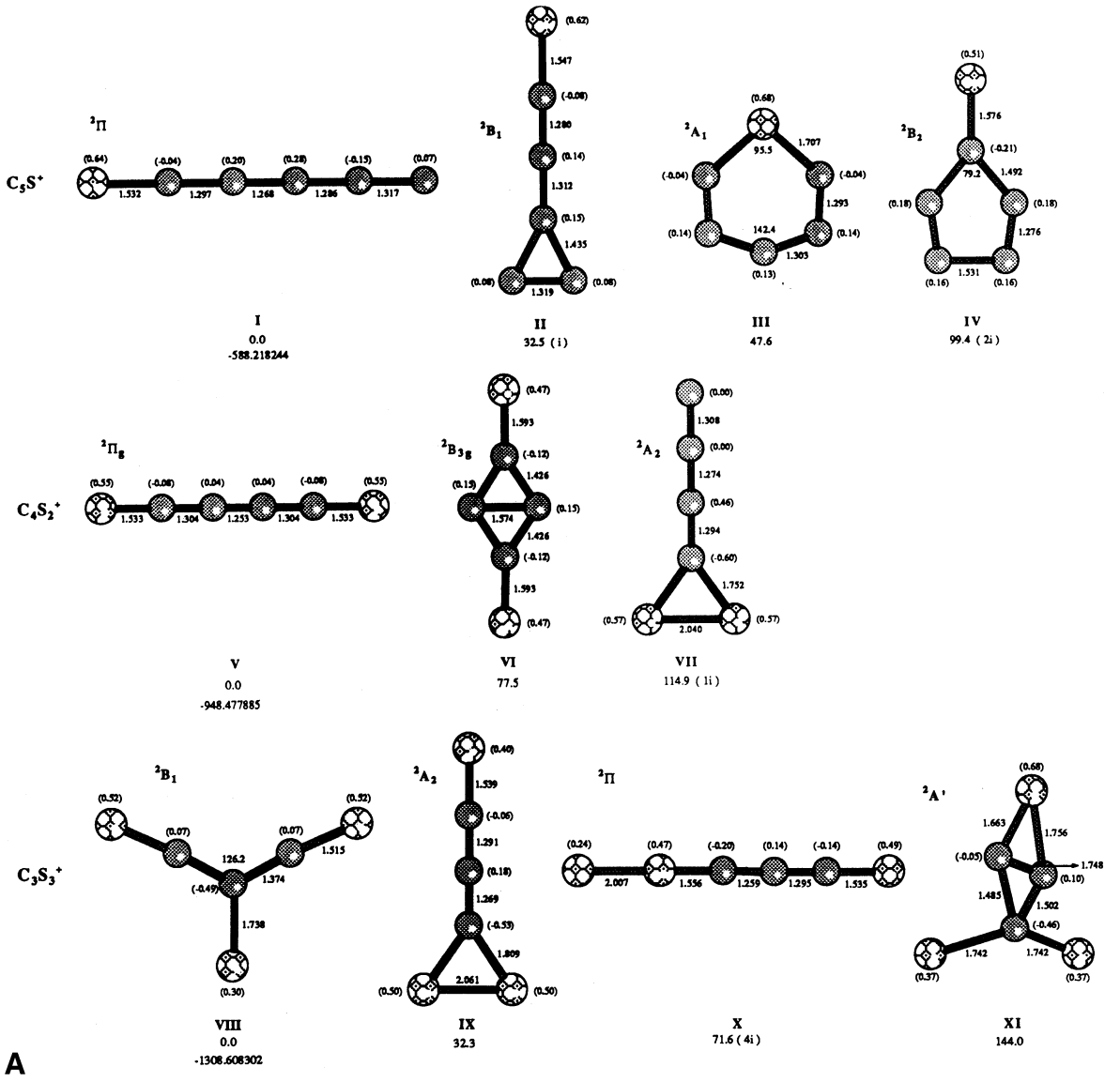

Fig. 8. Equilibrium geometries of $C_nS_p^+$ ($n + p = 6$) clusters at the B3LYP/6-311G* level of theory. Distances are in Ångstroms and angles in degrees. Mulliken charge distributions are given in parentheses. B3LYP relative energies (in kcal mol^{-1}) are displayed under each structure with some features about the vibrational frequencies (*r* indicates that all the frequencies are real, *i* notices one imaginary frequency, 2*i* two imaginary frequencies, etc.). B3LYP/6-311G* total energies (in hartree) are also reported under the global minimum of each compound.

Again, in these geometries, we can guess the association of two basic substructures, namely either (CS_3^+, S_2) or (S_3^+, CS_2) (Table 6). All these results can be rationalized by invoking that S easily partakes in double bonding with C rather than in linkage with other sulfur atoms, an effect that can ultimately break down a ring-shaped structure because the sulfur is essentially divalent in mixed carbon–sulfur clusters (the sulfur atom has six valence electrons but only two unpaired electrons, and the other two lone pairs do not participate into the bonding). Besides, S_6^+ is a truly six-membered molecule (D_{3d} hexagonal chair) with

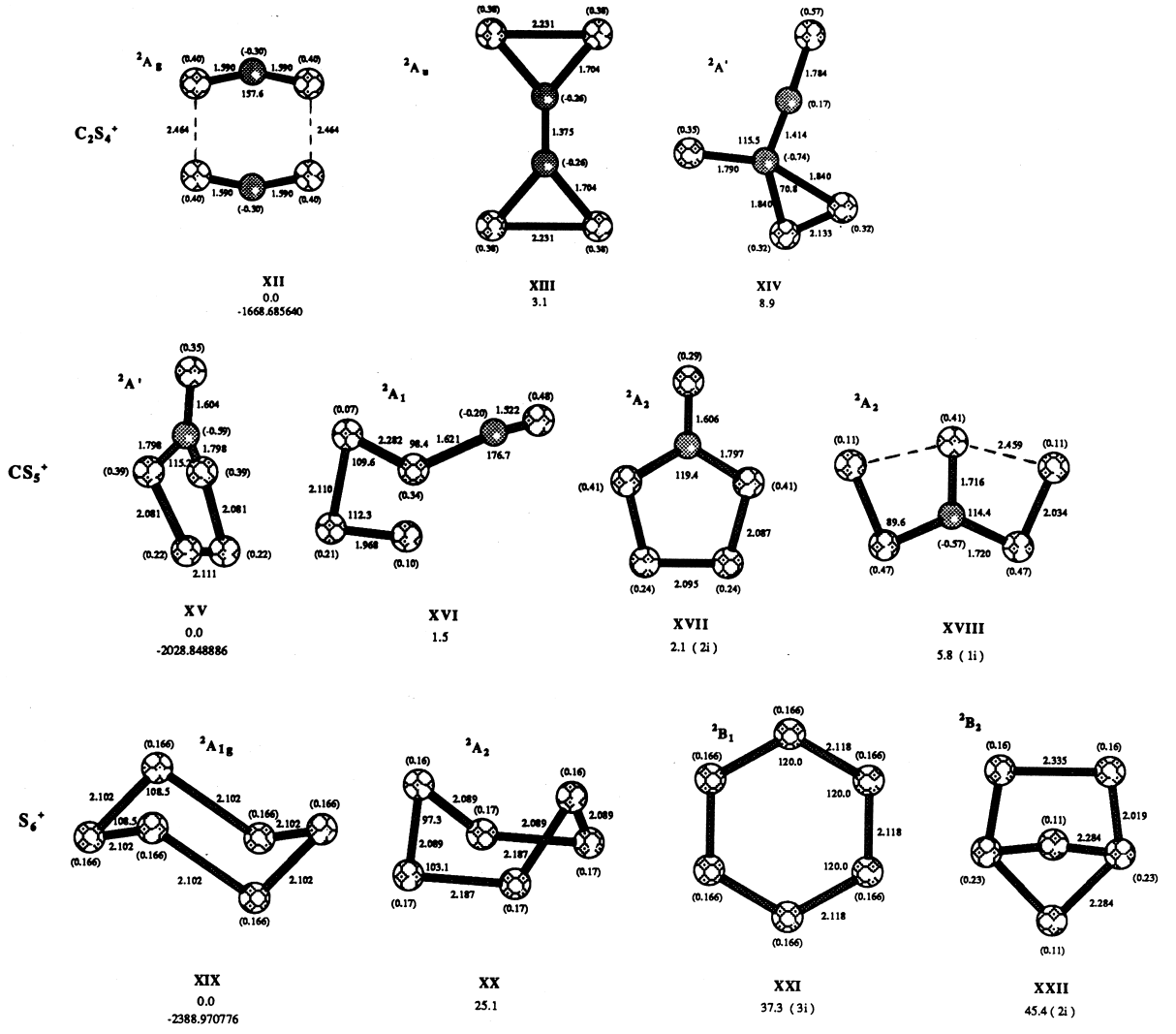

Fig. 8. (*continued*)

normal sulfur–sulfur single bond lengths (~2.10 Å). In a more general way, we can conjecture that the S_p^+ ($p = 4, 6, \ldots$) ring-shaped structures appear to be formed from two weakly interacting submolecules and become unclosed configurations as soon as one sulfur atom is replaced by a carbon atom in the cycle. This is because of the formation of two relatively strong SC double bonds, which then preclude the neighboring sulfur atoms involved in these SC bonds from associating with other adjacent sulfurs to close the cycle.

C. Geometry versus charge

The influence of the charge on geometry also deserves special attention because, in mass spectrometry, the clusters are ionized before analysis. Whether the cationic geometries can be expected to be relevant for the neutrals is thus an important question. For C_nSi_p ($n + p = 5, 6$), a comparison between the neutral and cationic forms clearly evidences that drastic change in the ground-state geometry can appear when the clusters are ionized. For instance,

Table 6
Building-up patterns of the $C_nS_p^+$ ($n + p = 5, 6$) clusters in their ground state

	ΔE_b (eV)
$C_2S_2^+$(linear, $^2\Pi_g$) + S(^{3}P) ↔ $C_2S_3^+$(VII, $^2A_1$)	2.06
CS_2^+(linear, $^2\Pi_g$) + *CS*($^1\Sigma^+$) ↔ *$C_2S_3^+$*(*VII*, $^2A_1$)	1.58
CS_2(linear, $^1\Sigma_g^+$) + S_2^+($^2\Pi_g$) ↔ CS_4^+(XI, $^2A_2$)	1.14
S_3^+(bent, $^2B_2$) + S_2($^3\Sigma_g^-$) ↔ S_5^+(XV, $^2A''$)	1.59
$C_3S_2^+$(linear, $^2\Pi_u$) + S(^{3}P) ↔ $C_3S_3^+$(VIII, $^2B_1$)	2.52
$C_2S_2^+$(linear, $^2\Pi_u$) + CS($^1\Sigma^+$) ↔ $C_3S_3^+$(VIII, $^2B_1$)	2.37
CS_2^+(linear, $^2\Pi_g$) + CS_2(linear, $^1\Sigma_g^+$) ↔ $C_2S_4^+$(XII, ^2A_g)*	−1.18
S_4^+(square ring, $^2B_{2u}$) + CS($^1\Sigma^+$) ↔ CS_5^+(XV, $^2A'$)	2.59
CS_3^+(T-shaped, $^2B_1$) + S_2($^3\Sigma_g^-$) ↔ CS_5^+(XV, $^2A'$)	1.66
S_3^+(bent, $^2B_2$) + CS_2(linear, $^1\Sigma_g^+$) ↔ CS_5^+(XV, $^2A'$)	1.05
S_3^+(bent, $^2B_2$) + S_3(bent, $^1A_1$) ↔ S_6^+(XIX, $^2A_{1g}$)	2.56
S_2^+($^2\Pi_g$) + $^2S_2$($^3\Sigma_g^-$) ↔ S_6^+(XIX, $^2A_{1g}$)	2.40
S_4^+(square ring, $^2B_{2u}$) + S_2($^3\Sigma_g^-$) ↔ S_6^+(XIX, $^2A_{1g}$)	1.37

* Metastable molecule.

Note. B3LYP/6-311G* total energies for S(^{3}P), $E = -398.132082$; CS($^1\Sigma^+$), $E = -436.246153$; CS_2($^1\Sigma_g^+$), $E = -834.550470$; CS_2^+($^2\Pi_g$), $E = -834.178372$; S_2($^3\Sigma_g^+$), $E = -796.412638$; S_2^+($^2\Pi_g$), $E = -796.057392$. The various structures, optimized with the B3LYP/6-311G* method, are reproduced in Figs. 7 and 8. ΔE_b denotes the binding energy of the cluster viewed as composed of the two submolecules listed in the first column.

C_3Si_3 prefers a three-dimensional structure [16], while $C_3Si_3^+$ adopts a Si-capped SiC_3Si bent chain [17]. The role of the charge in the geometry is hereafter examined for the C_nP_p and C_nS_p clusters. We have determined the ground-state geometry (global minimum) of each neutral C_nX_p (X = P, S; $n + p = 3$–6) clusters. To do that, as usual, several possible alternative geometric arrangements have been optimized. The resulting geometries are displayed in Figs. 9 and 10, respectively for X = P and S. When ionized, the C_nX and C_nX_2 species remain linear and tend toward the global minimum of the corresponding cation. Regarding the nonlinear forms, we find three categories: First, the geometry is not modified after ionization (if one excepts insignificant changes in the bond lengths and angles) and the ground-state geometries of both neutral and ionized structures are nearly identical. Such a situation is encountered in the mixed phosphorus–carbon clusters CP_3, C_2P_3, C_3P_3, CP_4, C_2P_4, and CP_5; in the mixed sulfur–carbon clusters CS_3, C_2S_3, and CS_4; and in the pure sulfur clusters S_3 and S_6.

Second, the geometry remains unchanged after ionization but the related arrangement of nuclei does not represent the global minimum of the cationic congener. This occurs when the geometry adopted by the neutral species in its ground state corresponds to a local minimum on the PES of the cation. Thus, P_3 is linear ($^2\Pi_g$), but this configuration is metastable for P_3^+ ($^3\Sigma_g^-$, structure XIV), being located at 39.5 kcal mol^{-1} above the ground state, namely a cyclic D_{3h} form ($^1A_1'$, structure XIII). Likewise, such a situation also exists in sulfur compounds. The global minimum of S_4 is predicted to be a singlet cis planar structure [34–36]. This open chain also corresponds to a minimum on the PES of the cationic parent S_4^+, but the global minimum in the latter one is represented by a square ring ($^2B_{2u}$, structure XIII), located under the cis open chain by 7.8 kcal mol^{-1}. A reverse situation appears in S_5. In the neutral S_5, the global minimum

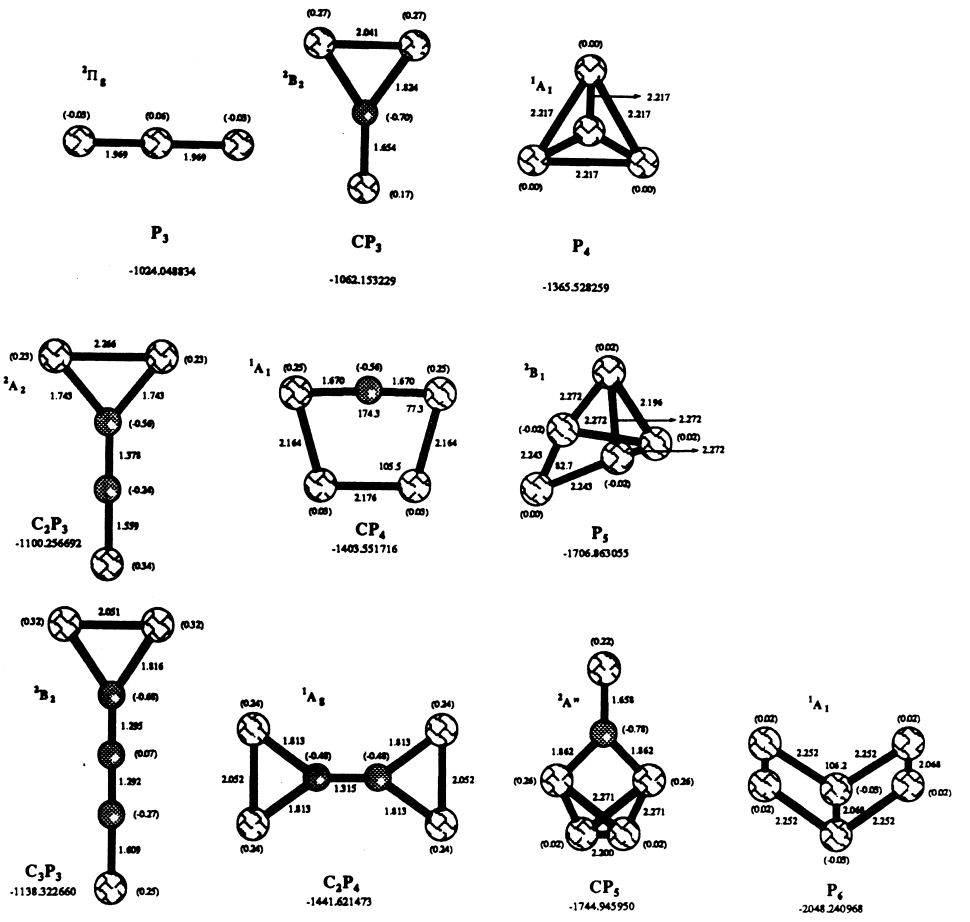

Fig. 9. Ground state geometries of neutral C_nP_p ($n + p = 3$–6) clusters. B3LYP/6-311G* total energies (in hartree) are displayed under each structure.

is a five-membered puckered ring, whereas in the related cation we find a cis-trans open chain ($^2A''$, structure XV) as ground state. In S_5^+, however, the energy separation between the open chain and the closed ring is found to be insignificant, on the order of 1 kcal mol^{-1}, and these two states eventually appear almost degenerate. A few mixed sulfur–carbon clusters also belong to this category, namely, C_3S_3 and C_2S_4 (Figs. 8, 10).

Third, the geometry is drastically changed after ionization. The latter situation appears when the ground-state geometry of the neutral species does not correspond to any local minimum on the PES of the monopositive ion. We find typical examples in the pure phosphorus cluster family. For instance, when ionized, the tetrahedral P_4 rearranges without activation to the global minimum of P_4^+, that is, the puckered ring-shaped form ($^2B_1$, structure XVII). Distortion to lower symmetry ($T_d \rightarrow C_{2v}$) causes considerable stabilization in this molecule (tetrahedral P_4^+ possesses three imaginary frequencies and is a saddle point of higher order on the PES). Another case of interest is the pure phosphorus cluster P_5. The neutral P_5 is a distorted tetrahedral P_4 edge capped by an additional phosphorus. After ionization, this structure directly evolves toward the global minimum of P_5^+, that is a perfect tetragonal pyramid ($^1A_1$, structure XVIII). Likewise, the neutral P_6 prefers a V-like arrangement of nuclei, which ultimately distorts to the puckered double-T-shaped configuration of the corre-

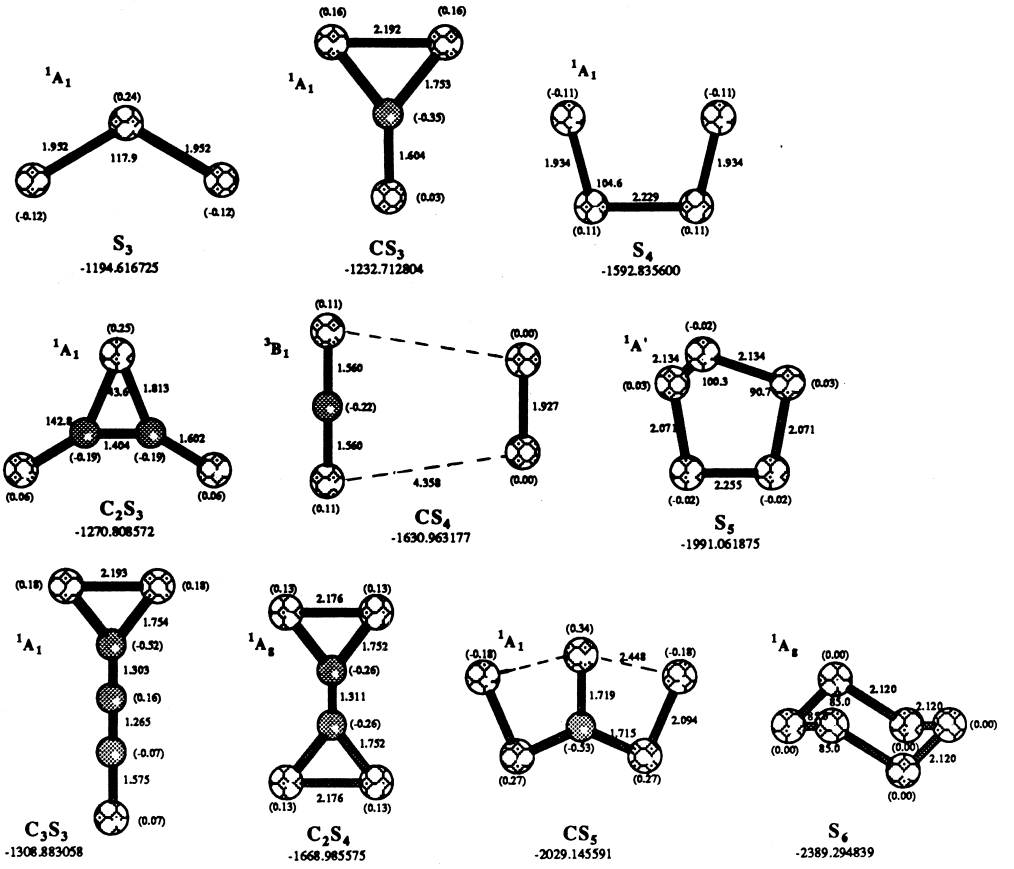

Fig. 10. Ground-state geometries of neutral C_nS_p ($n + p = 3$–6) clusters. B3LYP/6-311G* total energies (in hartree) are displayed under each structure.

sponding cation P_6^+ (^2A_g, structure XXIV), the V-like arrangement of nuclei ($^2A_1$, structure XV) being a saddle point on the PES of P_6^+.

4. Conclusion

A comparative study of cations $C_nX_p^+$ (X = P, S; $n + p = 3$–6) has been presented. General tendencies were derived as for the structural properties of these clusters. In particular, building-up patterns of medium-sized $C_nX_p^+$ clusters can be set up on a few simple rules, the most important being that CC bonds are favored over CX bonds that and XX bonds are avoided in mixed clusters. In carbon-rich structures, the heteroatoms (S or P) occupy the outermost positions relative to the pure carbon substructure. Because of the multivalence of phosphorus, the phosphorus-rich clusters can adopt various ground-state geometries. Besides, S remains divalent in mixed sulfur–carbon structures, strongly limiting the number of bonds that sulfur can form. As a matter of fact, sulfur-rich clusters very often appear in the form of Van der Waals complexes, and pure sulfur clusters are either rings (S_4^+, S_6^+) or open chains (S_3^+, S_5^+). Regarding the role of the charge in the relative stability of the atomic arrangement, either pure phosphorus or pure sulfur compounds (except S_3 and S_6) and a number of mixed sulfur–carbon clusters, namely, C_3S_3, C_2S_4, and CS_5, adopt distinct geometries depending on whether each of these clusters is in

its neutral or ionic form. This result is important in mass spectrometry techniques where the cluster is ionized before observation and measurement.

Acknowledgements

The Laboratoire de Physique des Lasers, Atomes et Molécules is Unité Mixte de Recherche de l'Université de Lille 1 et du CNRS 8523. The Centre d'Etudes et de Recherches Lasers et Applications (CERLA) is supported by the Ministère chargé de la Recherche, the Région Nord-Pas de Calais and the Fonds Européen de Développement Economique des Régions.

References

[1] C.-R. Wang, R.-B. Huang, Z.-Y. Liu, L.-S. Zheng, Chem. Phys. Lett. 242 (1995) 355.
[2] C.-R. Wang, R.-B. Huang, Z.-Y. Liu, L.-S. Zheng, Chem. Phys. Lett. 237 (1995) 463.
[3] T. Kimura, T. Sugai, H. Shinohara, Chem. Phys. Lett. 256 (1996) 269.
[4] J.L. Fye, M.F. Jarrold, J. Phys. Chem. 101 (1997) 1836.
[5] D.C. Parent, Int. J. Mass Spectrom. Ion Processes 116 (1992) 257.
[6] Y. Negishi, A. Kimura, N. Kobayashi, H. Shiromaru, Y. Achiba, N.J. Watanabe, J. Chem. Phys. 103 (1995) 9963.
[7] J.D. Presilla-Marquez, C.M.L. Rittby, W.R.M. Graham, J. Chem. Phys. 106 (1997) 8367; and references therein.
[8] D. McNaughton, D. McGilvery, F.J. Shanks, Mol. Spectrosc. 149 (1991) 458.
[9] Y. Oshima, Y. Endo, J. Mol. Spectrosc. 153 (1992) 627.
[10] J.M.L. Martin, P.R. Taylor, J. Phys. Chem. 100 (1996) 6047.
[11] M.L.J. Martin, J. El-Yazal, J.P. François, Chem. Phys. Lett. 242 (1995) 570.
[12] M. Ohishi, H. Suzuki, S. Ishikawa, C. Yamada, H. Kananori, W.M. Irvine, R.D. Brown, P.D. Godfrey, N. Kaifu, Asliophys. J. 380 (1991) L39.
[13] M.B. Bell, P.A. Feldman, S. Kwok, H.E. Matthews, Nature 295 (1982) 389.
[14] M. Ohishi, N. Kaifu, K. Kawaguchi, A. Murakami, S. Saito, S. Yamamoto, S. Ishikawa, Y. Fujita, Y. Shiratori, W.M. Irvine, Asliophys. J. Lett. 345 (1989) L83.
[15] M.B. Bell, L.W. Avery, P.A. Feldman, Asliophys. J. 417 (1993) L37.
[16] G. Froudakis, A. Zdetsis, M. Mühlhaüser, B. Engels, S.D. Peyerimhoff, J. Chem. Phys. 101 (1994) 6790.
[17] G. Pascoli, H. Lavendy, Int. J. Mass Spectrom. Ion Processes 177 (1998) 31.
[18] G. Pascoli, H. Lavendy, Int. J. Mass Spectrom. Ion Processes 189 (1999) 125.
[19] G. Pascoli, H. Lavendy, Int. J. Mass Spectrom. Ion Processes 181 (1998) 135.
[20] G. Pascoli, H. Lavendy, Int. J. Mass Spectrom. Ion Processes 173 (1998) 41.
[21] Gaussian 94, Revision C.3, Frisch, M.J.; Trucks, G.W.; Schlegel, H.B.; Gill, P.M.W.; Johnson, B.G.; Robb, M.A.; Cheeseman, J.R.; Keith, T.; Petersson, G.A.; Montgomery, J.A.; Raghavachari, K., Al-Laham, M.A.; Zakrzewski, V.G.; Ortiz, J.V.; Foresman, J.B.; Ciolowski, J.; Stefanov, B.B.; Nanayakkara, A.; Challacombe, M.; Peng, C.Y.; Ayala, P.Y.; Chen, W.; Wong, M.W.; Andres, J.L.; Replogle, E.S.; Gomperts, R.; Martin, R.L.; Fox, D.J.; Binkley, J.S.; Defrees, D.J.; Baker, J.; Stewart, J.P.; Head-gordon, M.; Gonzalez, C.; Pople, J.A.; Gaussian, Inc., Pittsburgh P.A. (1995).
[22] R. Krishnan, J.S. Binkley, R. Seeger, J. Pople, J. Chem. Phys. 72 (1980) 650.
[23] R.A. Kendall, T.H. Dunning Jr., R.J. Harrison, J. Chem. Phys. 96 (1992) 6796.
[24] T.H. Dunning, Jr., J. Chem. Phys. 90 (1989) 1007.
[25] A.D. Becke, J. Chem. Phys. 98 (1993) 5648.
[26] C. Lee, W. Yang, R.G. Parr, Phys. Rev. B 37 (1988) 785.
[27] K. Raghavachari, G.W. Trucks, J.A. Pople, M. Head-Gordon, Chem. Phys. Lett. 157 (1989) 479.
[28] G.E. Scuseria, T.J. Lee, J. Chem. Phys. 93 (1990) 585.
[29] H. Lavendy, J.M. Robbe, J.P. Flament, G. Pascoli, J. Chim. Phys. 94 (1997) 649.
[30] J. Novosad, in R.B. King (Ed.) Encyclopedia of Inorganic Chemistry, Vol. 6, p. 3144, Wiley, Chichester (England) 1994.
[31] H. Lavendy, J.M. Robbe, J.P. Flament, G. Pascoli, J. Chim. Phys. 94 (1997) 1779.
[32] H. Goldwhite, Introduction to Phosphorus Chemistry Cambridge University Press, Cambridge 1981.
[33] W.J. Hehre, L. Radom, P.V.R. Schleyer, J.A. Pople, Ab initio Molecular Orbital Theory, Wiley, New York 1986, Table 6.6.
[34] J.-L.M. Abboud, M. Esseffer, M. Herreros, O. Mó, M.T. Molina, R. Notorio, M. Yáñez, J. Chem. Phys. A 102 (1998) 7996.
[35] G.E. Quelch, H.G. Schaefer III, C.J. Marsden, J. Am. Chem. Soc. 112 (1990) 8719.
[36] K. Raghavachari, C.McM. Rohlfing, J.S. Binkley, J. Chem. Phys. 93 (1990) 5862.